ISEC 2024 – 3rd International Sustainable Energy Conference

Solar Thermal and Energy Efficiency for Sub-Saharan Africa‘s Industry and Commerce

https://doi.org/10.52825/isec.v1i.1168

Published: 29 Apr. 2024

Design and Economic Analysis of a Solar Thermal Pre-Cooling System for Agro-Cold Chain in Lesotho

Mpho Yengane[1*], Sebota Mokeke[1], and Moeketsi Mpholo[1]

[1] Energy Research Centre, National University of Lesotho, PO Roma 180, Lesotho

*Correspondence: Mpho Yengane, mphoyengane@gmail.com

Abstract. The agricultural sector in Lesotho grapples with significant challenges regarding post-harvest losses. Given that 40% of all agricultural products require cold storage, food quality is compromised due to lack of cold storage to extract the heat from exposure to high field temperatures after harvest. This research proposes a solar thermal cooling system tailored to the specific needs of preserving fresh agricultural produce, leveraging Lesotho’s abundant solar energy resources. Through TRNSYS simulation and MATLAB economic analysis, optimal system parameters are determined, ensuring both technical efficiency and financial viability.

The outcomes indicate that the proposed absorption solar thermal cooling system, incorporating evacuated tube collectors and an auxiliary boiler, effectively manages a cooling load of 7.318 kW, preserving fresh vegetables at 6.1°C. The optimized design features a chiller with a Coefficient of Performance of 0.8, a collector area of 12 m², and a hot storage volume of 0.2 m³, maximizing solar energy utilization. Importantly, economic metrics such as Levelized Cost of Energy ($0.085/kWh), Net Present Value ($9,200), Discounted Payback Period (12 years), and Savings to Investment Ratio (achieving 1 in year 13) demonstrate the financial feasibility and profitability of the system.

These findings underscore the potential of solar thermal cooling as a promising investment option for addressing refrigeration needs in Lesotho, offering a sustainable solution to mitigate post-harvest losses and enhance economic performance in the agricultural sector.

Keywords: Solar thermal cooling, Lesotho, Agricultural, Absorption cooling, TRNSYS, Coefficient of performance, Post-harvest losses, Economic analysis

1. Introduction

Since the 18th century, it has been acknowledged that food preservation is essential [1]. It is estimated that 40% of all agricultural products require cold storage [2]. Without cold storage facilities, farmers face a significant challenge in the form of post-harvest losses of perishable agricultural produce such as fruits and vegetables. This is primarily due to the metabolic processes that cause fresh produce to deteriorate and lose value. Fruits and vegetables can lose up to 20 hours of their shelf life due to field heat exposure [3]. In addition, perishable commodities are known to experience a faster deterioration rate as the temperature increases and the deterioration can increase two to three times with every 10 °C rise in temperature [4]. To ensure the quality and safety of perishable fruits and vegetables, storing them at their lowest safe temperature is critical.

In the past, reducing the moisture content of fresh vegetables was a common way to extend their shelf life. However, in the 21st century, consumers demand high-quality food, rendering this older practice limited [5, 6]. The need for fresh produce has driven early innovations in food storage technology, such as Smock and Neubert's research on controlled atmosphere storage of apples in 1950, which paved the way for groundbreaking advances in fresh food preservation and refrigeration [1]. Preserving food at high-quality levels requires a multi-dimensional chain system in which food is kept at low temperatures to slow down metabolic processes that lead to spoilage [2]. Since its inception, the refrigeration of fresh produce has continued to improve. In the early 2000s, this was accelerated by the increasing demand for premium quality fruits and vegetables, where global production witnessed significant growth, increasing by 30% from 1980 to 1990 and further by 56% from 1990 to 2003 [7, 8].

STC systems use solar energy to heat a secondary fluid, which flows through collectors to gain thermal energy and transfer it to the generator chamber of the chiller for the necessary condensation and evaporation processes that create the cooling effect. Solar thermal cooling (STC) systems have an advantage over solar photovoltaic (PV) systems in that they can harvest up to 98% of incident radiation and provide efficiencies of 60-70%, compared to solar PV panels that can only harvest up to 46% of visible light and offer a maximum efficiency of 20% [9]. However, a major obstacle to the growth of STC technology is its high initial cost and low overall system efficiency, making it difficult to currently compete commercially with conventional cooling technologies [10]. The surge in research on STC technology for air conditioning and refrigeration can be attributed to the energy crises of the 1970s; it also gained even more popularity in the early 90s as a solution to low electrification and off-grid cooling [11]. Two decades ago, a review by Best and Ortega on solar refrigeration and cooling found that the global system efficiencies achieved using evacuated tube collectors in conjunction with ammonia/water absorption systems were only 7-20%, depending on solar irradiation [12]. These efficiencies have since improved to 48% [13]. They also discovered that concentrating collectors are necessary for achieving lower temperatures ranging from 4 to 10°C. Furthermore, Brosnan suggests that swiftly pre-cooling agricultural produce to temperatures between 0 and 5 °C before transportation using STC can help prolong its shelf life by halting metabolic processes for 8 hours or more [14].

Reducing reliance on fossil fuel energy sources, which contribute to climate change, has been a significant driver in the development of STC technologies in the past two decades [15]. Absorption, adsorption, and desiccant cooling are the three most researched STC technologies. Still, they have not been able to provide consistent optimal cold storage temperatures and humidity levels of 0-12 °C and 80-95%, respectively, without an auxiliary heat supply [15, 16]. This is a major challenge in food refrigeration since maintaining steady temperatures and humidity is essential for optimal food quality. Nevertheless, the advantages of a solar thermal refrigeration system include low operating costs, no greenhouse gas emissions, and the ability to operate in remote areas without access to electricity.

Sub-Saharan Africa (SSA) has estimated 30-40% post-harvest food losses, which amounts to more than a third of all harvest [2, 7, 8]. These losses not only lead to financial difficulties for farmers but also discourage large-scale farming of perishable agricultural products, impeding the growth of the agriculture sector and exacerbating poverty and poor economic performance. This, in turn, leads to more deaths among children each year than the combined toll of AIDS, malaria, and tuberculosis [17]. In Lesotho, agriculture contributes 6.2% to the gross domestic product (GDP), and more than 70% of citizens depend on agriculture for food and income [16, 18–20]. It is therefore crucial for ensuring food security, economic growth, and development. Implementing post-harvest management systems such as cold room storage is crucial in reducing losses and shifting countries like Lesotho from food-deficient countries dependent on other countries to food-secure nations [3, 21]. Traditional cold rooms can be costly to purchase and maintain, which can increase storage expenses and decrease profit margins, particularly for small-scale farmers [5, 7]. Furthermore, these conventional cold rooms may not be easily accessible for off-grid usage near farming lands for pre-cooling purposes.

Nevertheless, the adoption of STC technologies remains limited in Lesotho probably due to a number of reasons including lack of awareness regarding their benefits, insufficient research, and limited financial resources.

This study revolves around the multifaceted exploration of solar thermal energy's applicability in refrigeration within the specific context of Lesotho. The research is driven by an intrinsic need to comprehend the potential advantages and challenges associated with the integration of solar thermal refrigeration systems. These considerations span various dimensions, including sizing, efficiency, and cost-effectiveness. The overarching goal is to shed light on the technical and socio-economic benefits stemming from the adoption of solar thermal refrigeration in the agricultural sector of Lesotho. Central to this endeavor is the design of STC system specifically tailored to address the unique challenges faced in Lesotho. Furthermore, the research encompasses a thorough economic analysis of the proposed model, evaluating its viability against conventional cooling systems.

The detailed objectives guiding the system design include:

- Conducting a comprehensive assessment of the current state of refrigeration in Lesotho, encompassing an analysis of demand, existing systems, and prevalent challenges.
- Evaluating the potential of solar thermal energy for refrigeration in Lesotho by considering factors such as solar resource availability, technological suitability, and integration prospects with the local infrastructure.
- Designing a solar thermal refrigeration system with a keen focus on efficiency, cost-effectiveness, and contextual appropriateness.
- Performing a robust economic evaluation to ascertain the tangible benefits of implementing solar thermal refrigeration in Lesotho.

These objectives are concretized within specific constraints of attaining pre-cooling temperatures ranging from 0-12 °C for identified agricultural products, including cabbage, tomato, green pepper, and green beans. The solar thermal refrigeration system will be designed to optimize key performance indicators, including high collector efficiency, a high coefficient of performance (COP), a high solar fraction, high exergy efficiency, and substantial primary energy savings. A comprehensive economic analysis is carried out, scrutinizing metrics such as the Levelized Cost of Energy (LCOE), Net Present Value (NPV), Savings to Investment Ratio (SIR), and Discount Payback Period (DPP) to determine the competitiveness and economic viability of the proposed solar thermal refrigeration system relative to conventional counterparts.

The design and economic analysis of a STC system in Lesotho are grounded in a multitude of justifications that highlight the potential advantages and positive impacts associated with the adoption of this innovative technology. Lesotho's compact size of 30,355 km^2 and the uniform distribution of solar irradiation levels ranging from 5.5-7.2 kWh/m^2, shown in Figure 1, position the country as an ideal location for the deployment of solar thermal absorption cooling systems. The solar radiation peak during the hottest hours of the day further aligns with the periods of peak cooling loads, thereby reducing the need for cooling during sunset or under cloudy conditions [22].

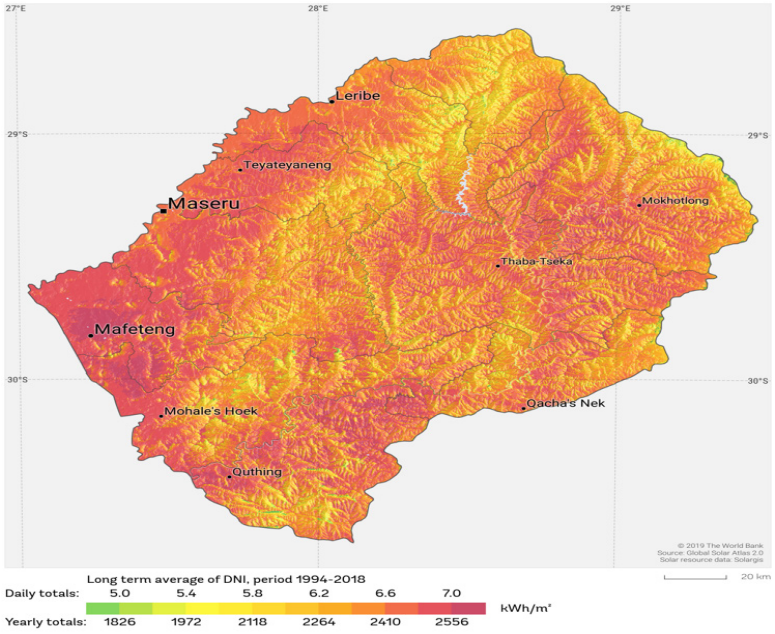

Figure 1. *Direct normal radiation patterns for Lesotho [22].*

Lesotho is heavily reliant on energy imports and it is imperative to reduce electricity demand by implementing solar thermal absorption cooling systems. Research by Wang in 2010 suggests that solar-assisted cooling systems could yield energy savings of 40-50% [23]. This is also supported by Ullah et al. [24]. This is a particularly pertinent consideration in the face of Lesotho's existing capacity shortage, with a national peak load of 203.48 MW and a domestic generation capacity of only 74.7 MW as of 2022 [25]. Additionally, projections by the International Energy Agency (IEA) anticipate a substantial drop in the total cost of STC systems by 35-45% by 2030 while grid electricity tariffs keep rising on an annual basis, emphasizing the imperative for increased investment STC technologies [26].

Despite advancements in electrification since the 2000s, less than half of Lesotho's population had access to electricity in 2020 as indicated in Figure 2 [4]. In 2024, there has barely been any improvement as access rate is only 51% from [27]. STC systems, capable of operating in rural areas not covered by the national grid, address disparities in access.

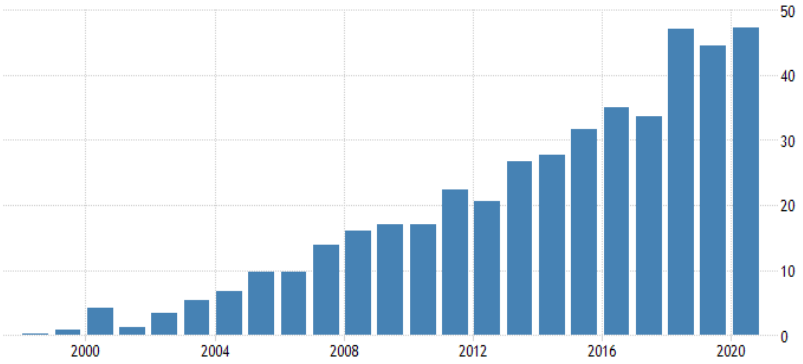

Figure 2. *Access to electricity in Lesotho by population percentage over 24 years [4]*

The rest of the paper is organized as follows: Section 2 describes the precise system of methods used as well as simulation technologies for STC in Lesotho's context. Section 3 provides results and discussion, where the STC simulation results are tabulated, analyzed, discussed, and criticized in reference to the literature. Section 4 is the conclusions and recommendations, where the main findings on the implemented STC technology are summarized, conclusions are drawn, and recommendations are presented for future research.

2. Methodology

This study focused on the pre-cooling of fresh vegetables which are a major source of food waste [28]. Pre-cooling temperatures of 0-12 °C for perishable vegetables were targeted, as recommended by the UN's Food and Agricultural Organization, FAO [29]. The cooling technology modeled in this study was absorption cooling. This is mainly due to its relatively high COP, low-pressure performance, relatively simple system design, and low maintenance [30]. TRNSYS was selected to perform the system simulation in this study. TRNSYS is a flexible modelling software that offers a graphical interface used to simulate transient systems' behaviour. Furthermore, the literature shows TRNSYS' superiority and robustness in simulating STC systems. Model validation studies have shown that the mean error between TRNSYS software simulation results and measured results on a real system is under 10%, owing to its extensive library of components [31, 32]. TRNSYS requires knowledge of the desired cooling capacity. Therefore, cooling load calculations were performed in the Danfoss Cool-Selector software which allows for the selection of other crucial inputs such as the dimensions of the cold room, the type of agricultural produce that will be stored in refrigeration, and the frequency of produce turnover.

The study was carried out using typical meteorological year (TMY) data for January, with Maseru as a case study. The daily solar irradiation data for Maseru is shown in Figure 1 while the monthly climatic conditions provided by Meteonorm are shown in Figure 3. The simulation accounts for only the weather conditions in January as the peak vegetable harvest month and the warmest month in Lesotho [33]. This selection ensures that the system is tested under the most demanding operating conditions, providing insights into its performance during the period of highest cooling demand. By focusing on the month with the highest cooling load, the economic analysis can accurately assess the system's financial feasibility and profitability during the critical period.

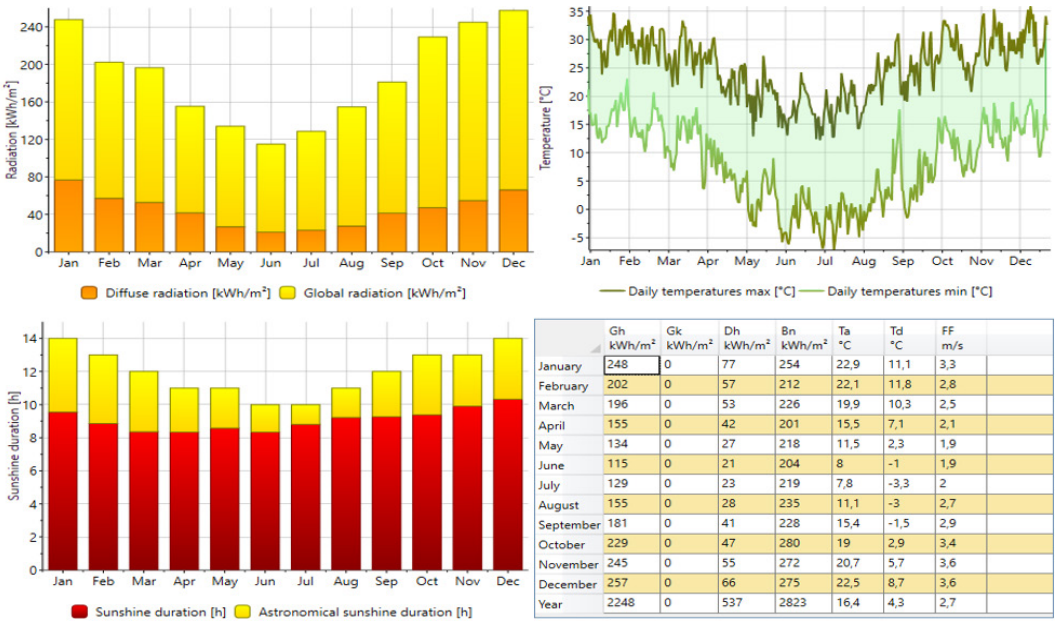

	Gh kWh/m²	Gk kWh/m²	Dh kWh/m²	Bn kWh/m²	Ta °C	Td °C	FF m/s
January	248	0	77	254	22,9	11,1	3,3
February	202	0	57	212	22,1	11,8	2,8
March	196	0	53	226	19,9	10,3	2,5
April	155	0	42	201	15,5	7,1	2,1
May	134	0	27	218	11,5	2,3	1,9
June	115	0	21	204	8	-1	1,9
July	129	0	23	219	7,8	-3,3	2
August	155	0	28	235	11,1	-3	2,7
September	181	0	41	228	15,4	-1,5	2,9
October	229	0	47	280	19	2,9	3,4
November	245	0	55	272	20,7	5,7	3,6
December	257	0	66	275	22,5	8,7	3,6
Year	2248	0	537	2823	16,4	4,3	2,7

Figure 3. *Monthly climate data for Maseru produced by Meteonorm.*

2.1 System configuration

The system consists of a solar thermal collector array, a hot water storage tank, a single effect absorption chiller, pumps, a refrigeration load, and an auxiliary boiler. The system configuration is shown in Figure 4.

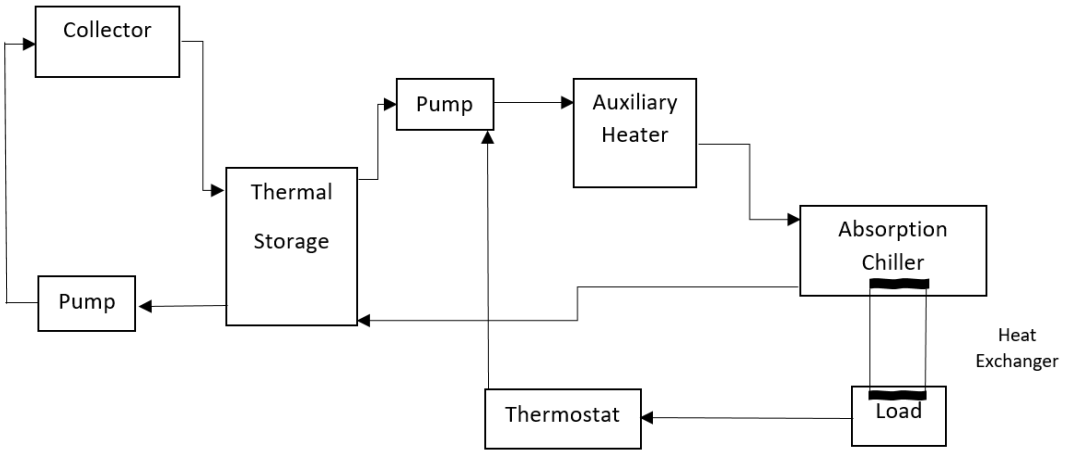

Figure 4. *STC system configuration.*

Water is pumped from the bottom of the stratified thermal storage tank through the collector array when the temperature of the collector array is greater than that of the storage tank outlet. Otherwise, the circulation through the collector array stops until its temperature is greater than the storage outlet temperature. Another pump is used to pump the hot water from the storage tank outlet towards the top of the storage tank through the auxiliary heater. The auxiliary heater is only turned on when the inlet water temperature is less than the set point temperature. It raises the water temperature to the set point temperature of 98 °C required as the heat supply for the absorption heater. The hot water coming into the absorption heater starts the absorption process and exits to return to the thermal storage tank. The absorption chiller's evaporator chamber is attached to the cooling load where heat is continuously absorbed from the load as cooling occurs. This keeps the temperature of the load at 6°C, which according to Asadi et al., is an adequate cooling temperature for cooling agricultural products [34].

2.2 Cooling load determination

The cooling load was modeled in Danfoss Cool-Selector. The cold-room design was such that it consisted of 75 mm thick polyurethane wall with a volume of 64 m^3 and mass capacity of 17,280 kg. This design was estimated to be adequate for the cold storage of agricultural produce from a smallholder farmer. The daily turnover of the cold produce was estimated to be 20% which amounts to 3,556 kg per day. The inlet temperature of 20 °C for fresh produce was based on the ambient temperature. The cold room was assumed to be built outside using a shipping container. Below-floor temperature and humidity were estimated to be 20 °C and 56%, respectively [35]. The desired temperature and humidity for the cold room were set to 6.1 °C and 95%, respectively. Some of the crucial design parameters of the cold room are summarized in Table 1.

Table 1. *Load determination (Danfoss).*

Calculated cold room load:	
Total cooling requirement	7.318 kW
Cold room details	
Temperature	6.1 °C
Relative humidity	95%
Operating hours	11.7 h
Dimensions	
Length	4 m
Width	4 m
Height	4 m
Stored goods	

Type	Vegetables
Quantity per day	3,556 kg
Inlet temperature	20 °C

The cooling system load profile relative to ambient temperature for January is shown in-Figure 5. The cooling load is expressed in TRNSYS as sensible load, which is the energy removed from the load through temperature reduction to facilitate chilling. It can be observed that during the day, when it gets warmer, the cooling load increases to a maximum of 26,270 kJ/h (7.3 kW), excluding the two extremes on the first and last day of January. This value is the system's peak cooling load. During the night, when it gets cooler and not much cooling is required, the cooling load decreases to 3,043 kJ/h (0.85kW), which is only 11.6% of the peak load.

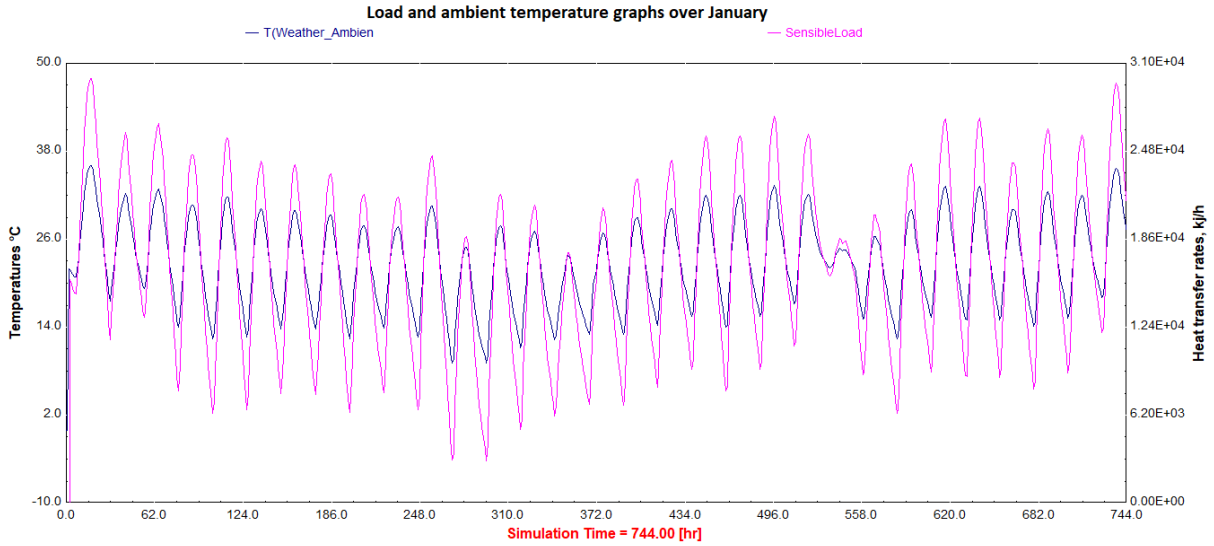

Figure 5. *Cooling system load profile variation with ambient temperature for January.*

2.3 TRNSYS modeling

The described solar thermal absorption cooling system was simulated using Maseru TMY weather data in TRNSYS. The freezing effects of the water used in the system were not considered since the target refrigeration temperature was 6.1°C. A full TRNSYS pictorial schematic of the cooling system is shown in Figure 6.

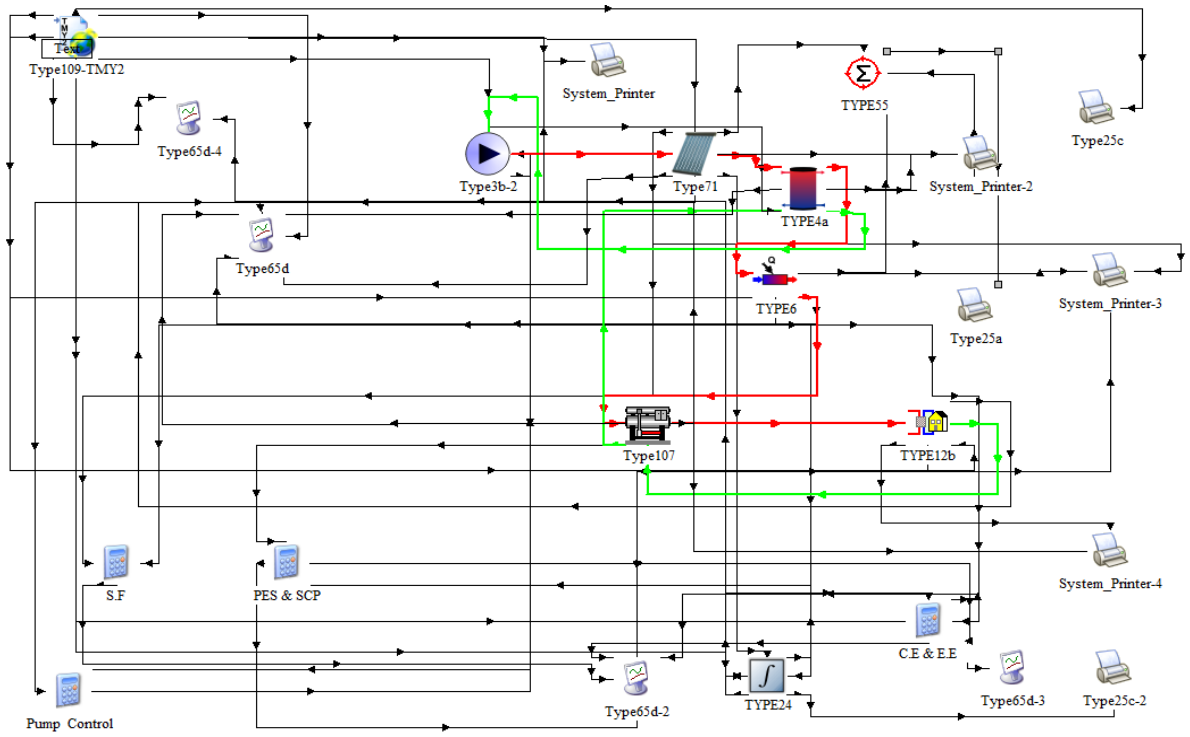

Figure 6. *TRNSYS STC system schematic.*

2.3.1 Absorption chiller

The absorption chiller used for the TRNSYS system simulation is a Type 107 hot water single-effect absorption chiller. Type 107 has a catalog data external file which predicts the chiller performance based on the inlet temperature of hot water ($T_{hw,in}$), chilled water set point ($T_{chw,set}$), and entering cooling water temperature ($T_{cw,in}$). The absorption chiller is modeled in three scenarios, all with a rated capacity of 73.318 kW and a rated COP of 0.5, 0.65, and 0.8. In this study, the chiller is operated at 10% capacity for a cooling load of 7.318 kW. To determine the energy delivered to the chiller by the hot water (Q_{hw}), the following equation is used:

$$Q_{hw} = \frac{C_{Rated}}{COP_{Rated}} f_{DesignEnergyInput} \quad (1)$$

Where $f_{designEnergyInput}$ is the actual current operating load, C_{Rated} is the chiller-rated capacity, and COP_{Rated} is the chiller-rated COP. The value of $f_{designEnergyInput}$ can be found in the absorption chiller external data file by first calculating the value of the fraction of the design load ($f_{designLoad}$) at which the chiller is required to operate. Then, the corresponding value of $f_{designEnergyInput}$ is determined concerning the inlet temperature of hot water, chilled water set-point, and entering cooling water temperature as shown in Figure 7.

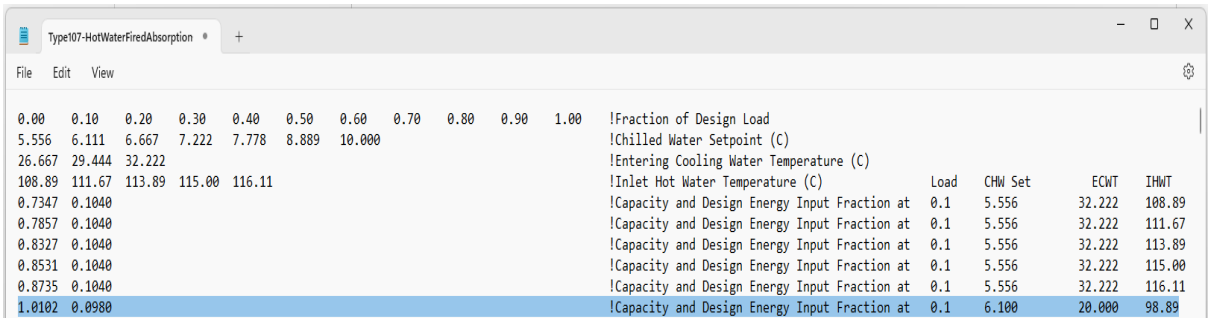
Type107-HotWaterFiredAbsorption

File Edit View

```
0.00   0.10   0.20   0.30   0.40   0.50   0.60   0.70   0.80   0.90   1.00   !Fraction of Design Load
5.556  6.111  6.667  7.222  7.778  8.889  10.000                             !Chilled Water Setpoint (C)
26.667 29.444 32.222                                                        !Entering Cooling Water Temperature (C)
108.89 111.67 113.89 115.00 116.11                                          !Inlet Hot Water Temperature (C)          Load  CHW Set  ECWT   IHWT
0.7347 0.1040                                                               !Capacity and Design Energy Input Fraction at  0.1   5.556   32.222  108.89
0.7857 0.1040                                                               !Capacity and Design Energy Input Fraction at  0.1   5.556   32.222  111.67
0.8327 0.1040                                                               !Capacity and Design Energy Input Fraction at  0.1   5.556   32.222  113.89
0.8531 0.1040                                                               !Capacity and Design Energy Input Fraction at  0.1   5.556   32.222  115.00
0.8735 0.1040                                                               !Capacity and Design Energy Input Fraction at  0.1   5.556   32.222  116.11
1.0102 0.0980                                                               !Capacity and Design Energy Input Fraction at  0.1   6.100   20.000  98.89
```

Figure 7. *Type 107 absorption chiller external data file.*

The following equation determines the value of $f_{designLoad}$.

$$f_{DesignLoad} = \frac{Q_{Remove}}{Capacity_{Rated}} \quad (2)$$

Where Q_{Remove} is the energy that must be removed from the chilled water stream to bring it from its entering temperature to the set point temperature which is equivalent to the cooling load.

The mass flow rate for chilled water entering the chiller can be determined using the following equation for the amount of energy to be removed from the chilled water stream.

$$Q_{Remove} = \dot{m}_{chw} Cp_{chw} (T_{chw,in} - T_{chw,set}) \quad (3)$$

Where $\dot{m}_{chw}$ is the mass flow rate of the chilled water, Cp_{chw} is the chilled water specific heat capacity, $T_{chw,in}$ is the inlet chilled water temperature, and $T_{chw,set}$ is the chilled water set point temperature.

Additionally, the following equation defines the chiller hot water stream outlet temperature. The equation is useful for finding the mass flow rates of the hot water stream and cold water stream when the hot water inlet temperature ($T_{hw,in}$), hot water outlet temperature ($T_{hw,out}$), hot water specific heating capacity (Cp_{hw}), and hot water energy (Q_{hw}) are already known.

$$T_{hw,out} = T_{hw,in} - \frac{Q_{hw}}{\dot{m}_{hw} Cp_{hw}} \quad (4)$$

The energy balance equation for the chiller shown in the following equation is used to determine the energy rejection to the cooling water stream (Q_{cw}).

$$Q_{cw} = Q_{chw} + Q_{hw} + Q_{Aux} \quad (5)$$

Where Q_{Aux} is the energy attributed by various parasitic energy consumers in the system such as solution pumps, fluid stream pumps, and controls. In this study, the parasitic energy consumption is assumed to be zero for simplicity.

The mass flow rate of the cold water stream can then be determined using the following equation:

$$T_{cw,out} = T_{cw,in} + \frac{Q_{cw}}{\dot{m}_{cw} Cp_{cw}} \quad (6)$$

Where $T_{cw,in}$ is the cold water inlet temperature, $T_{cw,out}$ is the cold water outlet temperature, Cp_{cw} is the cold water specific heating capacity, and Q_{cw} is the energy rejected to the cold water stream.

Type 107 absorption chiller is only applicable for catalog data sourced from different manufacturers' specifications. Therefore, input parameters for this absorption chiller have to be within operating limits. Table 2 shows the calculated input parameters for the Type 107 absorption chiller given different COP values.

Table 2. *Input parameters for TYPE 107 absorption chiller.*

Parameter	Description
Q_{remove}	7.318 kW
Q_{hw}	14.34 kW
Q_{cw}	21.66 kW
m_{chw}	628.75 kg/h
m_{hw}	1,232.08 kg/h

m_{cw}	1,846.68 kg/h
$f_{designLoad}$	0.1004
$f_{designEnergyInput}$	0.098

2.3.2 Solar thermal collectors

Type 71 evacuated tube solar thermal collectors were used in TRNSYS simulation to provide thermal energy for the cooling system. Since efficiency is essential in collector selection, the following thermal efficiency equation is used in TRNSYS to govern the performance of the collector.

$$\eta = a_0 - a_1 \frac{(T_i - T_a)}{G_T} - a_2 \frac{(T_i - T_a)^2}{G_T} \quad (7)$$

Where a_0, a_1, and a_2 are the thermal efficiency parameters representing the y-intercept, slope, and curvature of the collector efficiency versus temperature difference/radiation ratio curve, respectively. According to Quality Assurance in Solar Heating and Cooling Technology (QAiST), their values are given in Type 71 as 0.75, 0.832, and 0.0208, respectively [36]. The variables T_i and T_a are the collector inlet temperature and the ambient temperature, respectively.

2.3.3 Thermal storage tank

Type 4a stratified storage tank with uniform losses is used for this TRNSYS simulation. This is a hot water storage tank that stores the necessary thermal energy needed to reach the required 98 °C for regeneration in the chiller. Stratification of the storage tank improves system performance by lowering the return temperature of the solar collector which increases its efficiency and operating hours. Figure 8 shows the energy balance diagram for the storage tank.

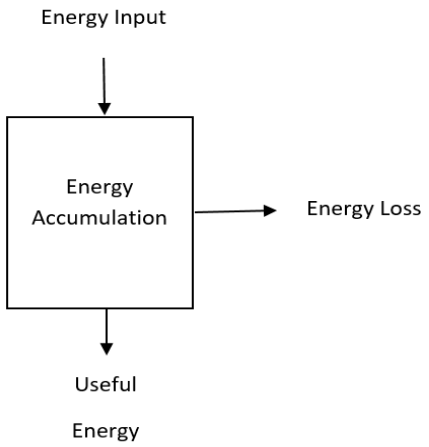

Figure 8. *Energy balance diagram for the hot water tank.*

2.3.4 Auxiliary heater

Type 6 auxiliary heater is incorporated into the system in TRNSYS simulation to provide auxiliary thermal energy for low irradiation periods to keep the cooling temperatures within the required limits. The auxiliary heater only turns on when the inlet fluid temperature is less than the set point temperature of 98 °C. Whenever the auxiliary heater is switched on, the following equation is used to model the heat energy (Q_{boiler}) required to increase the temperature of the heating fluid from the storage tank outlet temperature to the desired chiller inlet temperature. Whenever the auxiliary heater is switched on, the following equation is used to model the heat energy (Q_{boiler}) required to increase the temperature of the heating fluid from the storage tank outlet temperature to the desired chiller inlet temperature.

$$Q_{boiler} = mC_P(T_o - T_i) \quad (8)$$

2.3.5 Other TRNSYS components

The weather data is processed using the Type 109 Weather data reader and processor component of TRNSYS. The component is used to read and process weather data which includes solar radiation properties and ambient temperature for a given area as shown in Figure 9 and-Figure 10, respectively. It does this by calculating the incident radiation on the surface of the solar collectors which were tilted at 30° towards the north, with a surface azimuth angle of 0° and consideration of 0.2 ground reflectance [37].

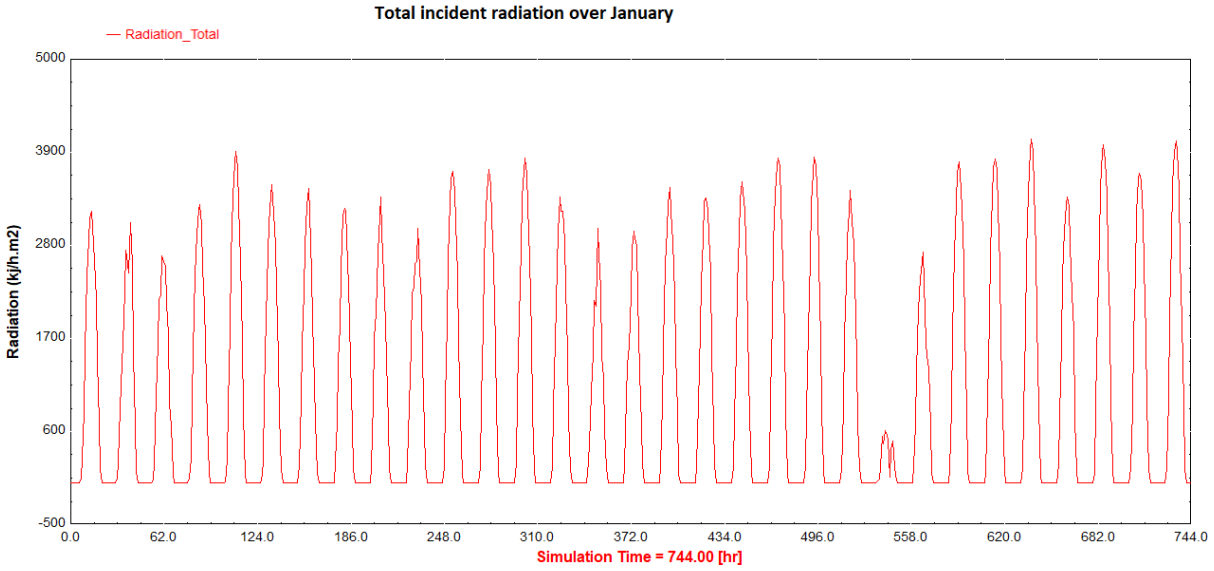

Figure 9. *Maseru radiation profile for January.*

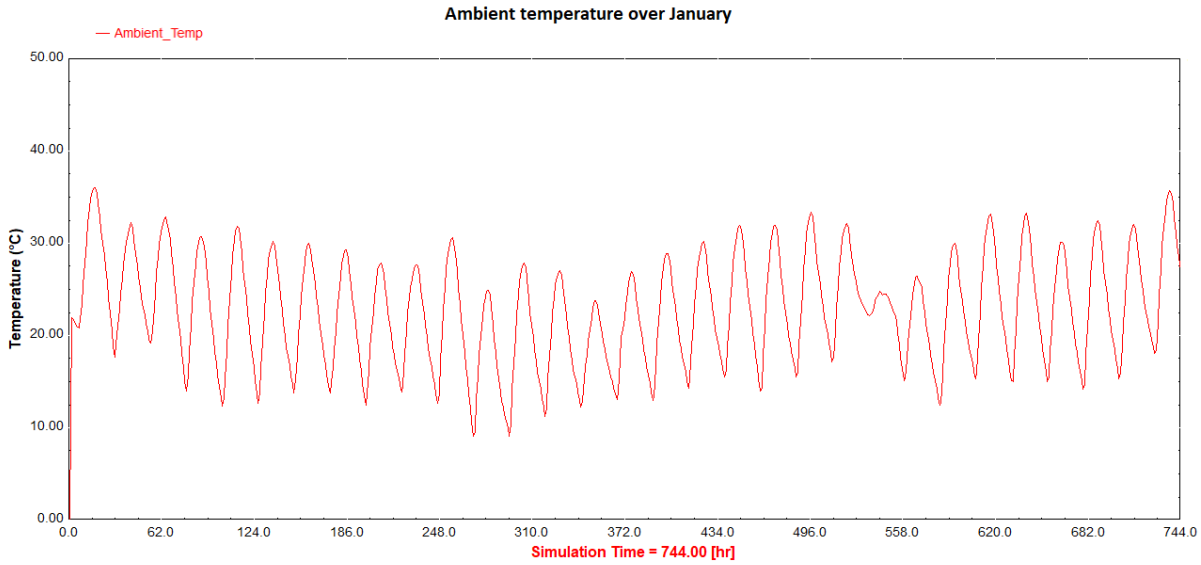

Figure 10. *Maseru ambient temperature for January.*

Supporting components used in the system include a Type 12b load, Type 3b-2 fluid pump, Type 65d online graphical plotter, Type 25 system printer, Type 24 quantity integrator, and Type 55 periodic integrator.

TRNSYS has several components that have different design parameters and the choice depends on factors such as the load for which it is designed and atmospheric conditions. Some of the most crucial TRNSYS system parameters are shown in Table 3.

Table 3. *Typical operating parameters used in TRNSYS modeling.*

Parameter	**Description**
Hot water single-effect absorption chiller	
Cooling load	7.318 kW
Chilled water set point	6.1 °C
Chilled water flow rate	628.75 kg/h
Hot water inlet temperature	98 °C
Hot water flow rate	1232.08 kg/h
Cooling water inlet temperature	20 °C
Cooling water flow rate	1846.68 kg/h
Solar collectors	
Fluid inlet flow rate	1232.08 kg/h
Slope	30°
Storage tank	
Tank type	Stratified
Hot side and cold side flow rate	1232.08 kg/h
Fluid density	1000 kg/m^3
Auxiliary heater	
Set point temperature	98 °C

2.4 System performance metrics

In this TRNSYS simulation, collector efficiency is measured monthly and seasonally. This collector efficiency (η) is expressed as the ratio of the useful gain (Q_{useful}) over a specific period to the incident radiation (G_T) and collector area (A_c) over the same defined period as shown in the following equation:

$$\eta = \frac{\int Q_{useful}}{A_c \int G_T} \tag{9}$$

The periodical (monthly or seasonal) solar fraction (SF) was computed in TRNSYS to determine the contribution of solar energy to the system using Equation (10).

$$SF = \frac{\int Q_{sun}}{\int Q_{sun} + \int Q_{boiler}} \tag{10}$$

Where, Q_{boiler} is the thermal energy received from the auxiliary boiler and Q_{sun} is the thermal energy received from the sun.

Primary energy savings is computed in TRNSYS using Equation (11). The reference system is an electrically operated absorption chiller. Variables Q_{boiler} and $Q_{cooling,ref}$ are the heat energy provided by the auxiliary boiler, and the cooling energy supplied by the conventional refrigerating system, respectively. The variables η_{boiler}, ε_{heat}, and ε_{el} are the efficiency of the boiler, the conversion efficiency of fossil fuel supplying the boiler, and the heat-providing electricity efficiency, respectively. COP_{ref} is the rated efficiency of the absorption chiller.

$$PES = 1 - \frac{\left(\frac{\int Q_{boiler}}{\varepsilon_{heat}\eta_{boiler}}\right)}{\left(\frac{\int Q_{cooling,ref}}{COP_{ref}\varepsilon_{el}}\right)} \tag{11}$$

The term inside the brackets in Equation (11) is the ratio of the primary energy consumption of a solar thermal system contributed by an auxiliary boiler to the primary energy consumption of a reference absorption system using traditional energy sources to meet the same load. The values of ε_{heat}, ε_{elec}, and COP_{ref} were estimated as 0.7, 0.4, and 1.0 [38].

The exergy efficiency of an absorption chiller can be defined as the ratio of the actual cooling output to the maximum possible cooling output that could be obtained if the chiller operated at Carnot efficiency between the source and sink temperatures. Exergy efficiency is sometimes referred to as the second-law efficiency and is used to evaluate the effectiveness of the system relative to an idealized or reversible system equivalent [39]. This is a more comprehensive comparison, giving a more realistic representation of the system's efficiency. Exergy efficiency considers not only the energy quantity, but also its quality from a thermodynamic perspective. The exergy efficiency of an absorption chiller can be calculated using Equation (12).

$$\eta_{exergy} = Q_c * \eta_{Carnot} \tag{12}$$

Where Q_c is the cooling output demand and η_{Carnot} is the Carnot efficiency. The Carnot efficiency for cooling can be calculated using Equation (13):

$$\eta_{Carnot} = \left(\frac{T_a}{T_c}\right) - 1 \tag{13}$$

Where T_c is the temperature of the cooling medium and T_a is the ambient temperature.

The most crucial performance indicator for the absorption chiller is the coefficient of performance, defined in TRNSYS as:

$$COP = \frac{Q_{chw}}{Q_{aux}+Q_{hw}} \tag{14}$$

Where Q_{chw} is the energy removed from the chilled water stream, Q_{aux} is the energy drawn by parasitic energy consumers, and Q_{hw} is the energy removed from the hot water stream.

2.5 Economic analysis

The financial analysis encompasses several key steps, starting with data from the TRNSYS simulation to obtain the necessary input parameters. Data was gathered on solar radiation levels, system performance characteristics, capital costs, operational and maintenance expenses, and discount rates. With this data, mathematical models that estimate electricity generation, operating costs, and financial indicators were developed. The implementation of the economic feasibility study involved leveraging MATLAB's capabilities to perform the required calculations.

Table 4 shows all the parameters used in determining the economic metrics. To determine the LCOE, NPV, SIR, and DPP for solar thermal absorption systems, the following method was employed. The lifetime for these systems is assumed to be 20 years. The discount rate applied was 7.75% equivalent to the Central Bank of Lesotho's average prime lending rate [40]. The capital cost per kW was estimated at $6,000 as typical for cooling systems, and since the system capacity is 7.318 kW, the total initial investment required was, therefore, $42,828. Additionally, the annual operational and maintenance cost was estimated to be 4% of the capital cost each [41]. The annual returns for the solar thermal absorption systems were determined based on the energy savings achieved for each COP simulation. To calculate these annual returns, the energy savings resulting from each COP simulation were quantified. Once the energy savings were estimated, they were multiplied by the 2023/2024 Lesotho general-purpose electricity tariff rate of M1.9624 ($0.053) to determine the corresponding annual financial returns [42].

Table 4. *Relevant parameters used in economic analysis.*

Parameter	**Value**
System Lifetime	20 years
Discount rate	7.75%

Initial investment	$ 42,828
Annual operation cost	4%
Annual maintenance cost	4%

Firstly, the Total Capital Cost (TCC) is calculated by multiplying the system capacity with the capital cost per kW. This provides an estimate of the total investment required for the system. Subsequently, the annual operation and maintenance cost is determined by taking 4% of the TCC. These costs represent the ongoing expenses associated with the system. The Annual Energy Production (AEP) is calculated based on the annual average solar irradiance in Lesotho, which is 2000 kWh/m^2, multiplied by the system capacity [43]. This estimation indicates the annual energy output that the solar thermal absorption system is expected to generate.

To calculate the LCOE, the present value of the O&M costs and the present value of the energy production were needed. The present value of the O&M costs was obtained by discounting the annual O&M cost over the system lifetime using the chosen discount rate. Similarly, the present value of the energy production is obtained by discounting the AEP over the system's lifetime. The LCOE is then determined using Equation (15).

$$LCOE = \frac{Lifetime\ Cost}{Lifetime\ Energy\ Production} = \frac{\sum_{t=1}^{n} \frac{I_t + M_t + F_t}{(1+r)^t}}{\sum_{t=1}^{n} \frac{E_t}{(1+r)^t}} \quad (15)$$

Where I_t is the investment expenditure, M_t is the operational and maintenance expenditures, F_t is the fuel expenditure, E_t is the cooling output, r is the discount rate, and n is the expected lifetime of the system. These variables, except for n, are accounted for over a year.

The NPV wass calculated using Equation (16). The present value of the annual returns is obtained by discounting the projected annual returns based on different COP simulations (0.5, 0.65, and 0.8) over the system lifetime.

$$NPV = -C + \sum \frac{(R-O)}{(1+d)^t} \quad (16)$$

Where C is the initial capital cost of the STC system, R is the annual energy cost savings generated by the system, O is the annual operating cost of the system, and d is the discount rate which represents the opportunity cost of investing in the system, and t is the year of the cash flow.

The SIR was obtained by using Equation (17). This ratio indicates the financial attractiveness of the project, with a higher SIR value indicating a more favourable investment.

$$SIR = \frac{NPV}{C} \quad (17)$$

Where C is the initial capital cost of the STC system.

Lastly, the DPP was determined by identifying the year in which the cumulative cash flow becomes positive using Equation (18).

$$DPP = t + \frac{C - \sum \frac{F_t + 1}{(1+t)^t}}{\sum \frac{F_t + 1}{(1+t)^t}} \quad (18)$$

Where t is the year when the cumulative discounted cash inflows from energy cost savings first exceed the initial investment cost of the system, C is the initial capital cost of the STC system, F_t is the net cash flow in year t (equal to the energy cost savings minus the

operating cost of the system), and *d* is the discount rate which represents the opportunity cost of investing in the system. The denominator of the equation represents the discounted cash inflows from energy cost savings generated by the system after the payback period, while the numerator represents the remaining discounted cash outflows required to recover the initial investment cost.

3. Results

3.1 TRNSYS analysis

Three different scenarios were simulated with three different absorption chillers having COP rated at 0.5, 0.65, and 0.8. The cooling load was determined by Danfoss Cool-Selector software as 7.318 kW.

3.1.1 Solar fraction

The solar fraction which represents the fractional contribution of the solar thermal collectors to the system's energy demand serves as one of the primary metrics for evaluating the cooling system's effectiveness. In cases where the solar fraction is not equal to one (1), the additional energy needed is provided by the auxiliary boiler. The results obtained from the TRNSYS simulation of a solar thermal absorption cooling system using different collector areas shown in Figure 11 provide valuable insights into the system's performance and its ability to meet cooling demand using solar energy for three different chiller-rated COP values (0.5, 0.65, and 0.8).

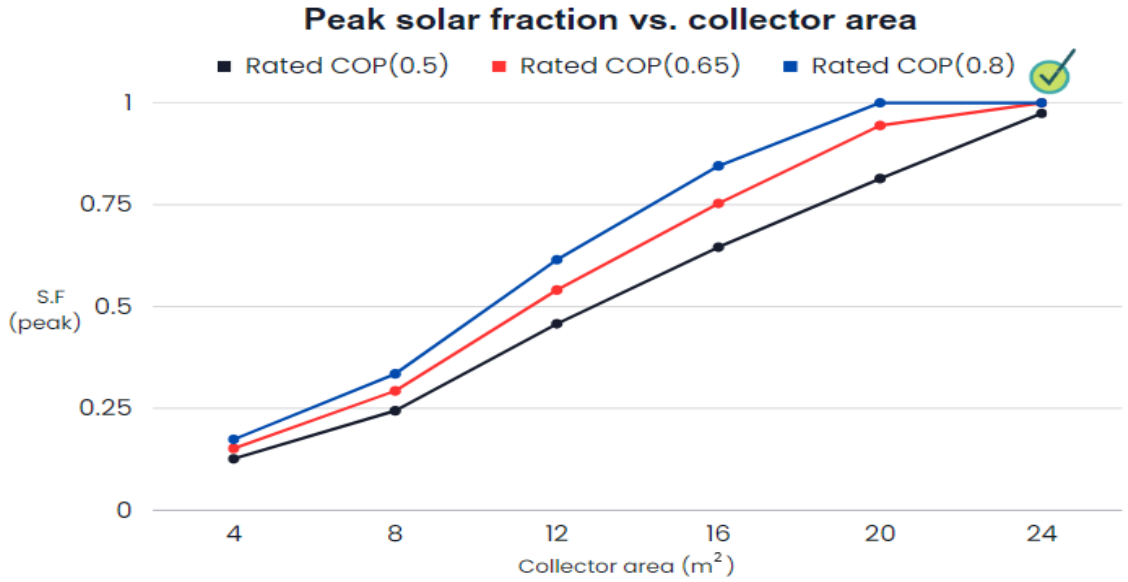

Figure 11. *Variation of solar fraction with collector area for the system.*

Starting with the simulation with a rated chiller COP of 0.5, when the collector area was 4 m^2, the solar fraction was found to be 0.1258, indicating that the solar thermal system can meet approximately 12.58% of the cooling load. As the collector area increased to 8 m^2, the solar fraction also increased to 0.2441, representing a significant improvement in system performance.

With further increases in the collector area to 8 m^2, 12 m^2, 16 m^2, and 20 m^2, the solar fraction increased to 0.4576, 0.6457, 0.8140, and 0.9743, respectively. The solar fraction values over January for the chiller rated COP of 0.5 and collector area of 12 m^2 are shown in Figure 12. These results demonstrate a substantial enhancement in the system's efficiency and its ability to meet a larger portion of the cooling load through solar energy utilization. This

aligns with the findings in a parametric study of a solar absorption cooling system by Sokhansefat et al. [44]. Sokhansefat et al. used evacuated tube collectors, a single-effect absorption chiller, an auxiliary heater, and a storage tank.

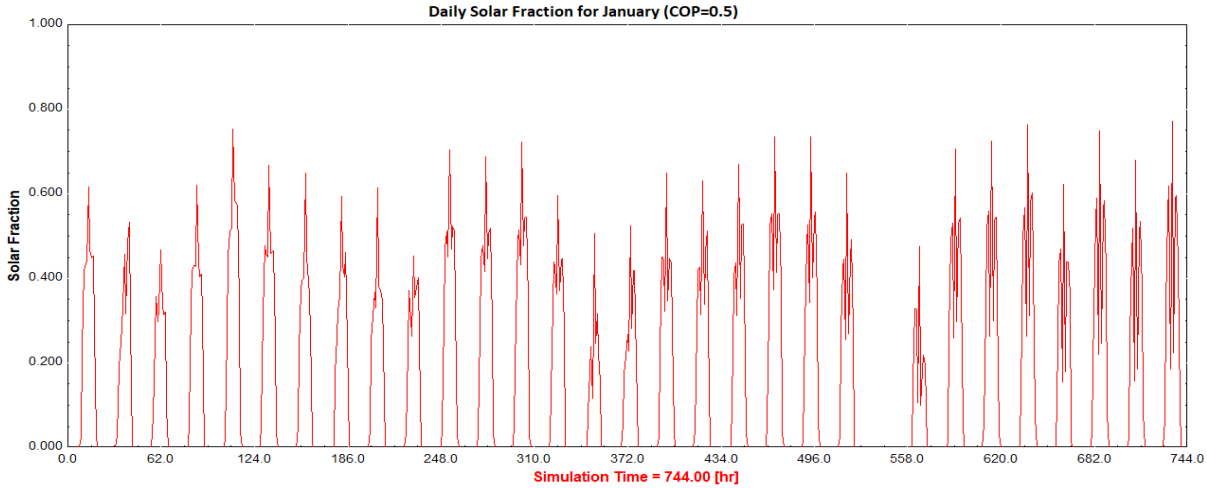

Figure 12. *Hourly solar fraction for January when rated COP is 0.5.*

When the rated chiller COP was 0.5, the solar fraction values were relatively low compared to the other two cases. This suggests that the chiller's efficiency was relatively low, requiring a larger portion of the cooling load to be met by non-solar sources. When the rated chiller COP was increased to 0.65 and 0.8, higher solar fraction values for all collector areas were observed. This indicates that the more efficient chiller allows the solar thermal system to supply a greater proportion of the cooling load. The solar fraction graphs over January for the rated COP of 0.65 and 0.8 are shown in Figure 13 and Figure 14, respectively.

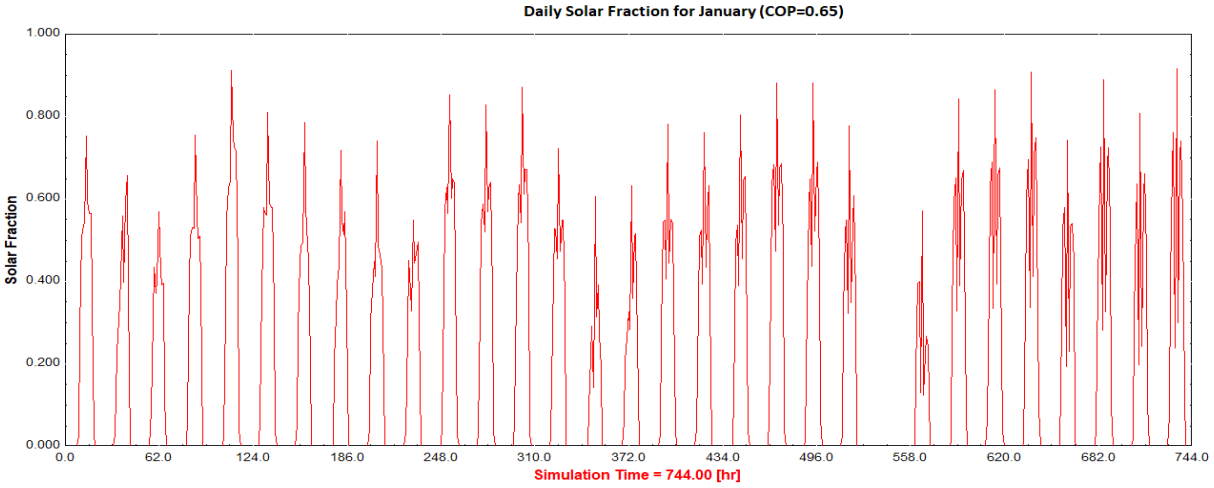

Figure 13. *Hourly solar fraction for January when rated COP is 0.65.*

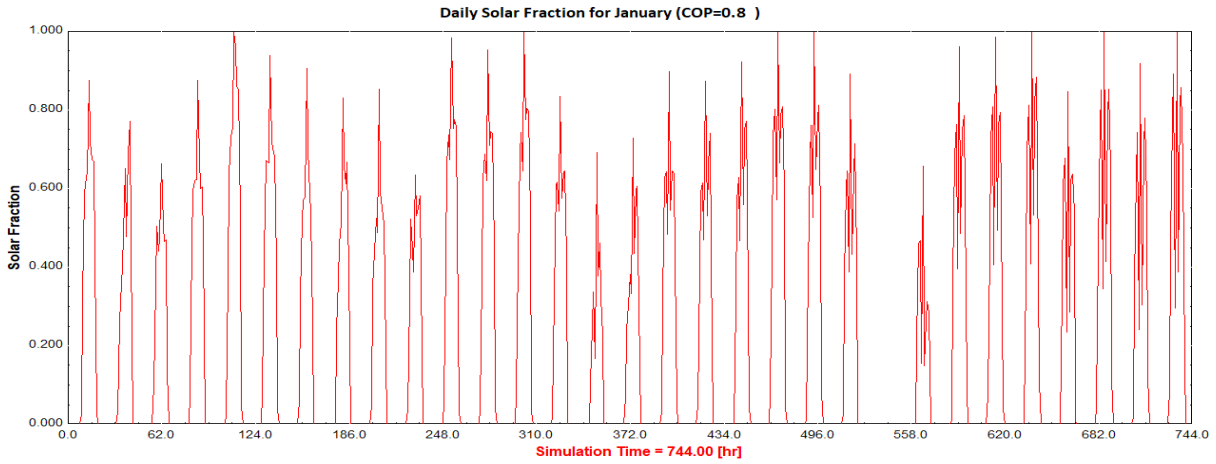

Figure 14. *Hourly solar fraction for January when rated COP is 0.8.*

Furthermore, with a collector area of 12 m^2, the solar fraction for the system with a chiller-rated COP of 0.8 reached its maximum value of 1. This implies that the solar thermal system can fully meet the cooling load using solar energy alone with collector temperatures up to 111 °C as shown in Figure 15, achieving the optimal system sizing for the given conditions. Achieving a solar fraction of 1 is highly desirable as it signifies complete reliance on renewable energy sources for cooling needs. This is consistent with findings by Uçkan and Yousif confirming that the evacuated tube collectors can reach the solar fraction of 1 in the absorption cooling [45]. In their study, Uçkan and Yousif used TRNSYS to determine the effect of various solar collector types on a solar absorption cooling system. While the trends observed are similar, it is worth noting that the system sizes are not comparable as Uçkan and Yousif achieve a solar fraction of 1 with an evacuated tube collector area of 140 m^2 to support a cooling capacity of 35 kW.

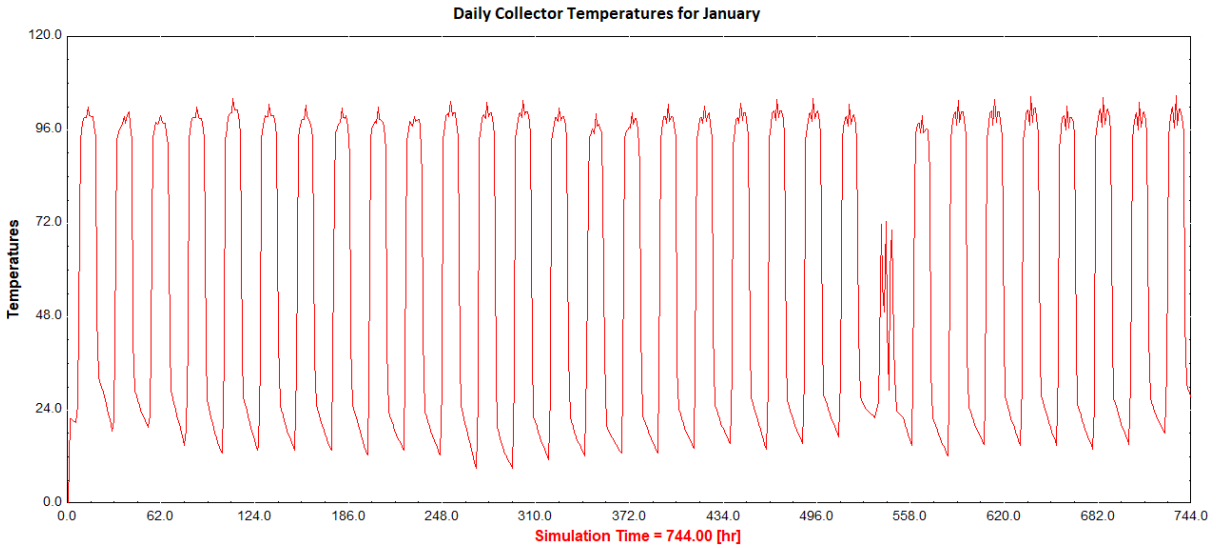

Figure 15. *Hourly collector outlet temperatures for January.*

The solar fraction values obtained for the different collector areas (4 m² to 24 m²) exhibit an increasing trend, which is generally expected, as can be seen in findings by Eicker and Pietruschka in their design of solar-powered absorption cooling systems [46]. However, the augmentation rate appears to diminish as the collector area gets larger. This trend is due to factors such as diminishing returns, system losses, and limitations in system efficiency. Nevertheless, across all three cases (rated COP of 0.5, 0.65, and 0.8), a general trend is observed a general trend where increasing the collector area leads to higher solar fractions.

This shows a positive correlation between the collector area and solar fraction in a solar thermal absorption cooling system. A larger collector area allows for the capture of more solar energy, leading to a higher solar fraction and increased utilization of solar thermal energy for the cooling system. However, it is important to consider other factors such as cost and available space.

3.1.2 Collector efficiency

The system's performance in terms of collector efficiency response to different collector slopes is shown in Figure 16.

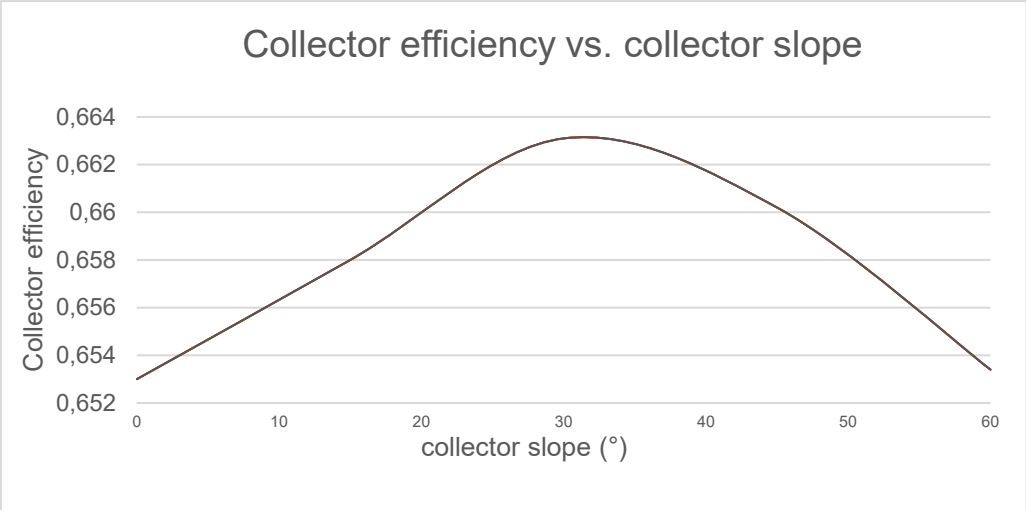

Figure 16. *Collector efficiency graphs for collector slopes.*

The results presented reveal the collector efficiency at various slope angles (0°, 15°, 30°, 45°, and 60°) for a solar thermal system in Maseru, Lesotho. The corresponding efficiency values for each slope angle are 0.653, 0.658, 0.6631, 0.6592, and 0.6534, respectively. These results demonstrate a slight variation in collector efficiency as the slope angle changes. The observed trend aligns with the expected behaviour of solar collectors and the influence of slope angle on efficiency. It is important to note that the collector efficiency peaked at a slope angle of 30°, which is closer to the optimal angle associated with the latitude of Maseru (29.3°).

At a slope angle of 0° (horizontal), the collector efficiency was 0.653. This relatively low efficiency can be attributed to reduced solar radiation absorption when the collector is parallel to the ground. In this position, the collector surface receives sunlight at a less optimal angle, resulting in lower energy capture and efficiency. The decrease in efficiency is due to the reduced exposure of the collector surface to the sun's rays, leading to decreased energy absorption. As the slope angle increased to 15° and 30°, the collector efficiency gradually improved, peaking at 30°. This trend can be explained by the increased alignment of the collector surface with the incident radiation as the slope angle approaches the optimal angle. At these angles, more solar radiation is incident on the collector surface, resulting in enhanced energy capture and higher efficiency. The improved alignment allows for better utilization of the available solar resource throughout the day, thus maximizing energy absorption. However, at a slope angle of 45° and 60°, the collector efficiency decreased slightly to 0.6592 and 0.6534, respectively. This decline can be attributed to the steeper slope angle which misaligns with the optimum incident radiation angle, hence limiting the energy absorption and decreasing the overall efficiency.

Additionally, it is noteworthy that the observed trends in collector efficiency remain consistent for different COP values (0.5, 0.65, and 0.8). This indicates that the COP does not directly influence collector efficiency as it primarily relates to the performance of the entire system, including components beyond the collector itself. Considering Maseru's latitude of

29.3°, it is expected that the collector efficiency would be higher at a slope angle closer to this latitude. The alignment of the collector surface with the sun's rays at a slope angle of 30° which is in proximity to the latitude, leads to higher energy capture and increased efficiency. This alignment ensures a more optimal angle of incidence for solar radiation throughout the year.

3.1.3 Primary energy savings (PES)

The fractional PES variation with the increasing collector area for the rated COP of 0.5, 0.65, and 0.8 are shown in Figure 17. The PES metric was simulated relative to a conventional electrical compression system.

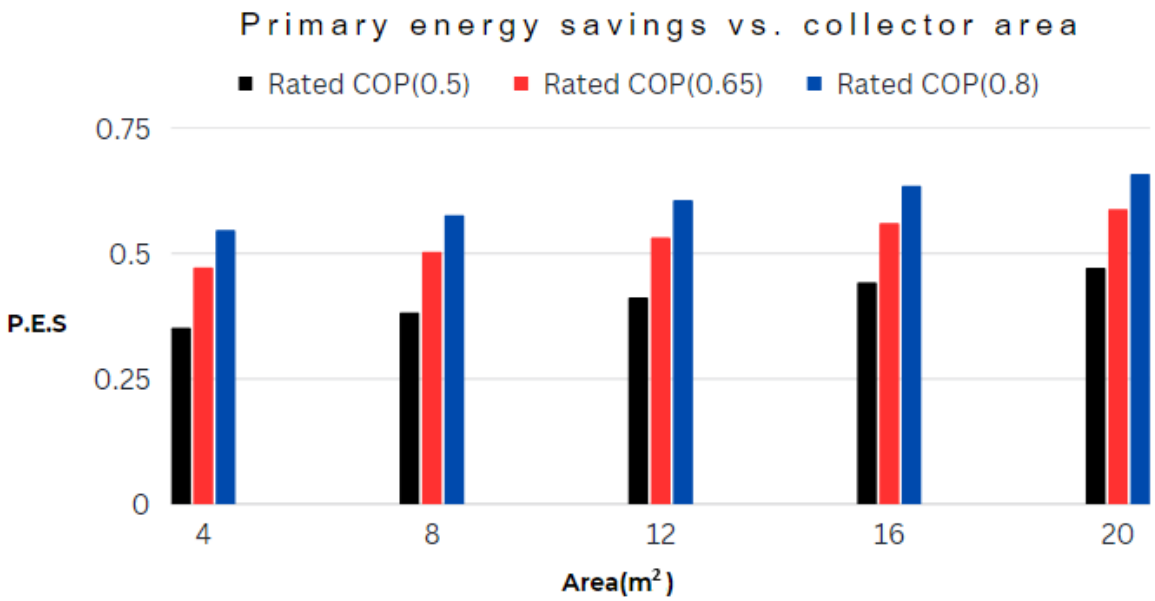

Figure 17. *Monthly primary energy savings for different collector areas for January.*

For a rated COP of 0.5, when powering the system with a collector area of 4 m^2, the simulation results yielded fractional primary energy savings of 0.3517. This indicates that the solar thermal absorption cooling system could achieve approximately 35.17% monthly primary energy savings compared to a conventional electrical compression system. Having increased the collector area to 8 m^2, the fractional primary energy savings increased to 0.3826, indicating a higher level of monthly energy savings. This suggests that a larger collector area substantially reduces the primary energy consumption compared to the conventional electrical compression system. With further increases in the collector area to 12 m^2, 16 m^2, and 20 m^2, the fractional primary energy savings continued to improve with values of 0.4123, 0.4418, and 0.4707, respectively. These results highlight the enhanced performance of the solar thermal absorption cooling system as the collector area increases, emphasizing the importance of larger collector areas for achieving significant primary energy savings.

For the COP of 0.65 and 0.8, the same trend was observed with the increasing collector area, and better yet, with much larger energy savings for higher COP. Energy savings observed for the rated chiller COP of 0.65 and 0.8 were 34% and 54% higher than those observed for the rated chiller COP of 0.5. This increase in energy savings due to an increase in COP can further be corroborated in Figure 18, Figure 19, and Figure 20. It can be observed that less auxiliary energy is required for a higher-rated COP. When the COP was 0.5, 0.65, and 0.8, the required auxiliary energy was 36,425 kJ/h, 29,092 kJ/h, and, 24,595 kJ/h respectively.

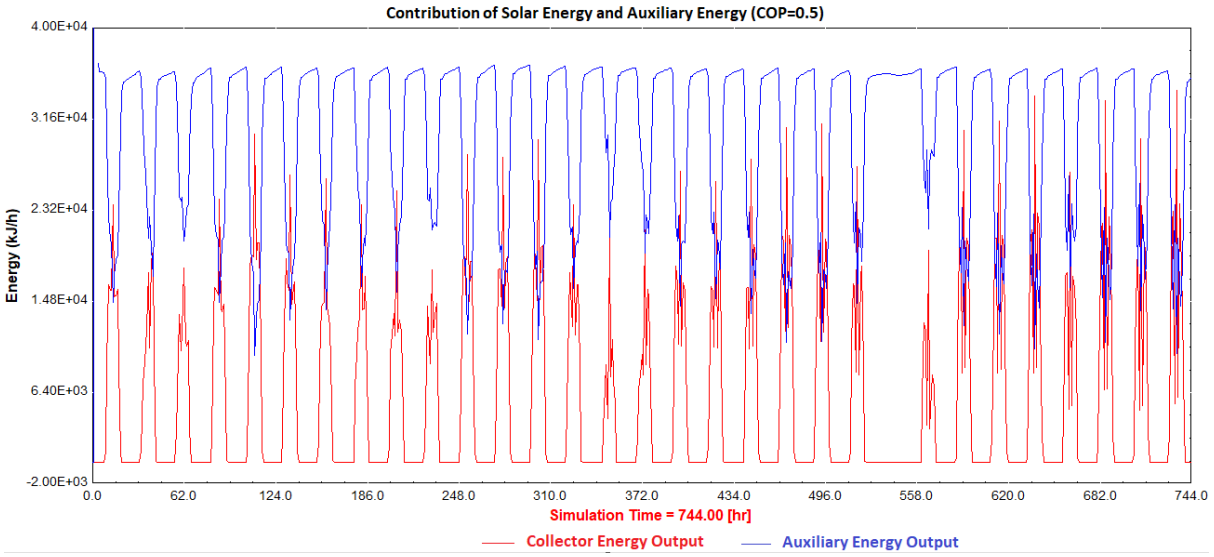

Figure 18. *System contribution of collector and auxiliary energy for rated COP of 0.5.*

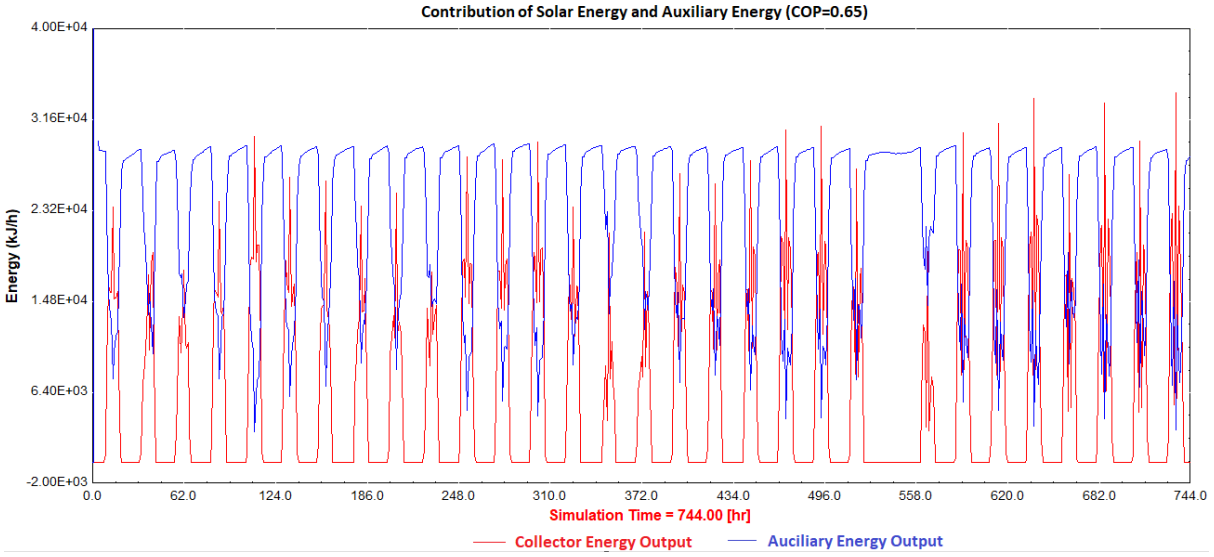

Figure 19. *System contribution of collector and auxiliary energy for rated COP of 0.65.*

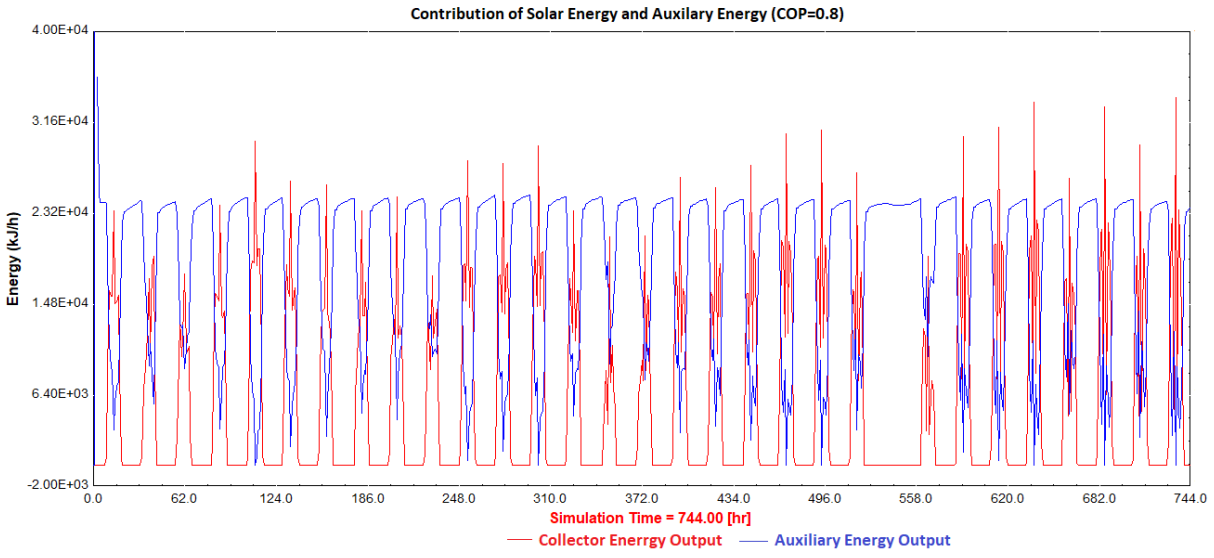

Figure 20. *System contribution of collector and auxiliary energy for rated COP of 0.8.*

The simulation results make apparent the positive impact of increasing the collector area and COP on the fractional primary energy savings of a solar thermal absorption cooling system. Larger collector areas enable the system to capture more solar energy, resulting in higher energy savings and reduced reliance on conventional electrical compression systems. These results are congruent with the findings by Figaj et al. in the feasibility study of a small-scale hybrid dish/flat-plate solar collector system as a heat source for the absorption unit [47]. Their design supported a 17 kW cooling load. They used the optimum concentrator area of 1.6 m^2 per kW of the nominal cooling power of the absorption chiller which is similar to the designed solar thermal absorption system for a 12 m^2 collector area and observed 50% primary energy savings. Additionally, a larger COP value implies that the absorption chiller can provide a greater amount of cooling while consuming less energy, signifying a more effective utilization of the heat source and efficient conversion of energy into cooling.

The results shown in Figure 21 are obtained from simulations of a solar thermal absorption cooling system considering the different chiller-rated COP values and varying hot storage volumes.

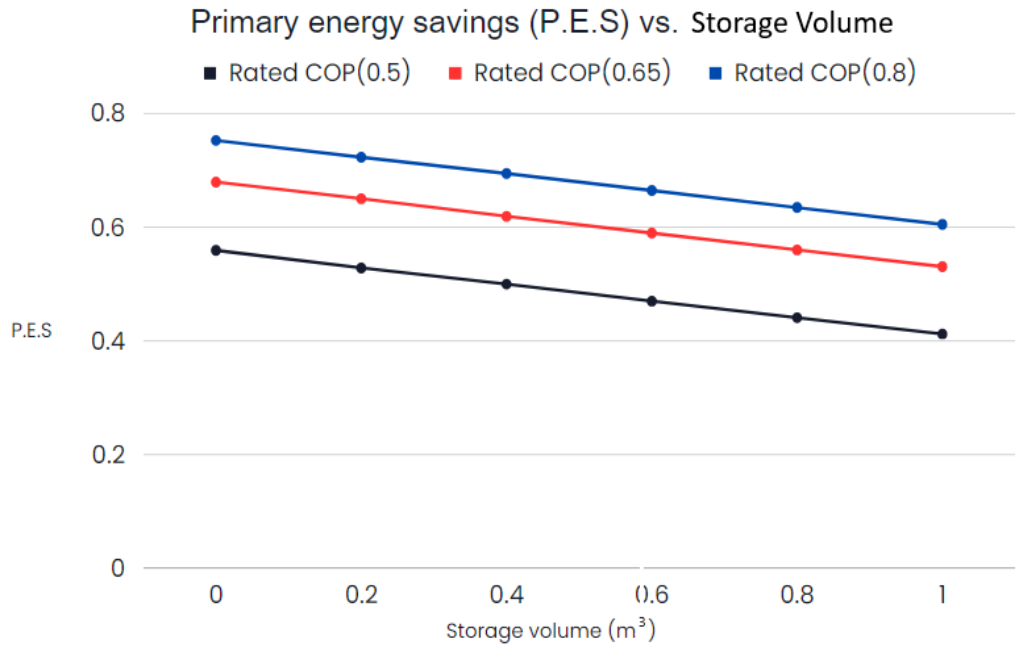

Figure 21. *Primary energy savings variation with hot storage volume.*

The system was first simulated for a rated chiller COP of 0.5. Without hot storage volume, the fractional primary energy savings of 0.5596 were observed. This result indicates that the system achieves approximately 55.96% monthly energy savings compared to the conventional electrical compression cooling system which was used as the reference. With a hot storage volume of 0.2 m^3, 0.4 m^3, 0.6 m^3, 0.8 m^3, and 1 m^3, the fractional primary energy savings decreased to 0.5286, 0.5002, 0.4702, 0.4411, and 0.4123, respectively. This suggests that the system achieves approximately 52.86%, 50.02%, 47.02%, 44.11%, and 41.23% energy savings compared to the reference. The simulation results demonstrate that as the hot storage volume increases, the primary energy savings of the solar thermal absorption cooling system decrease. This suggests that there is an optimal balance between the direct utilization of solar thermal energy and storage capacity for maximizing energy savings.

With a higher chiller-rated COP of 0.65, the primary energy savings are generally higher compared to the COP of 0.5, and for a chiller-rated COP of 0.8, the primary energy savings are significantly higher compared to the previous two cases. However, the trend remains the same, with the increasing hot storage volume leading to reduced energy savings. The highest

savings are achieved without thermal storage, and as the storage volume increases, the energy savings decrease. This is because larger thermal storage systems typically have higher standby losses

3.1.4 Exergy efficiency

The exergy efficiency indicates the effectiveness of the system in converting available energy into useful cooling, taking into account the quality of the energy and the irreversibilities within the system. Figure 22 shows the relationship between the chiller-rated COP and the exergy efficiency.

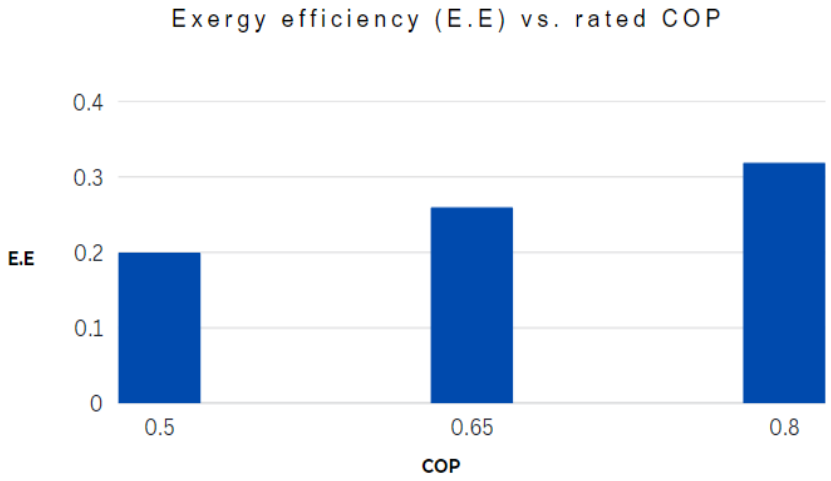

Figure 22. *Exergy efficiency for different values of collector area.*

Simulations were conducted with an elevated chiller-rated COP of 0.5, 0.65, and 0.8 yielding an increased exergy efficiency of 0.1992, 0.2591, and 0.3189, respectively. This discernible improvement suggests a more effective conversion of the available exergy input into useful work or cooling, demonstrating enhanced energy utilization capabilities within the system. Furthermore, Asadi et al. have provided supporting evidence for the validity of these results in their thermo-economic analysis and multi-objective optimization of absorption cooling systems driven by various solar collectors [34]. They found a closely similar exergy efficiency value of 0.236 and COP of 0.66 for 10 kW while using evacuated tube collectors for a cooling load of 10 kW. Furthermore, these findings align with those by Aman et al. in the energy and exergy analysis of an absorption cooling system in Canada. Their cooling load was 10 kW and they used chiller generator temperatures up to 90 °C, achieving the exergy efficiency of 0.32 [48]. Their slightly higher exergy efficiency is likely due to lower ambient temperatures in Canada. As the ambient temperature increases, the temperature difference decreases, resulting in a decrease in the Carnot efficiency. The Carnot efficiency represents the maximum possible efficiency of a heat engine operating between two temperature reservoirs. It is given by the temperature difference between the hot and cold reservoirs.

3.2 Economic impact analysis

MATLAB was used for the economic impact analysis of the STC system to determine the cost implication and economic feasibility of the system. Four economic metrics (LCOE, NPV, SIR, and DPP) were evaluated for different system technical performance metrics to find a balance between performance and economic viability.

The obtained results demonstrate that the LCOE for the solar thermal absorption cooling system is influenced by the rated COP as shown in Figure 23.

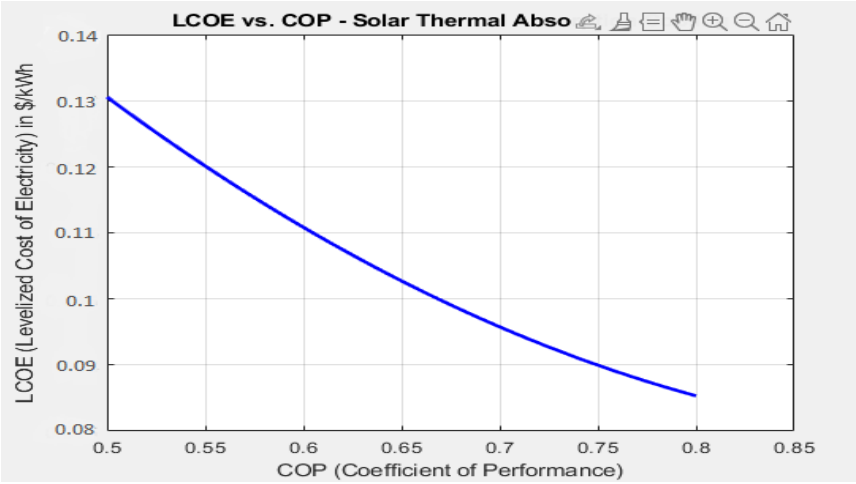

Figure 23. *LCOE for variation for different COP values (0.5, 0.65, and 0.8).*

Specifically, for a rated COP of 0.5, the LCOE was determined to be $0.13/kWh. As the rated COP increases to 0.65, a reduction in LCOE was observed, resulting in a value of $0.103/kWh. This reduction signifies that electricity production costs decrease as the system's COP improves. Furthermore, at a rated COP of 0.8, the LCOE further declines to $0.085/kWh, underscoring the cost-effective nature of the system under higher COP values. A lower LCOE of $0.039/kWh was observed by Ayadi and Al-Dahidi with COP of 0.79 [49]. This could be due to economics of scale as their cooling capacity was much higher at 160 kW.

These findings highlight the significance of higher COP values in achieving lower LCOE for the solar thermal absorption cooling system. The increase in COP signifies enhanced energy efficiency, leading to substantial cost savings in system operation. A higher COP indicates that the system can deliver more cooling per unit of input energy, resulting in reduced operating costs, and consequently, a lower LCOE. Drawing a comparison between these LCOE values and the average electricity cost of $0.10/kWh for refrigeration in Lesotho, several noteworthy observations arise: The first is, the solar thermal absorption cooling system demonstrates a less economical LCOE ($0. 0.13/kWh) at the lowest COP of 0.5 compared to the prevailing average electricity cost of $0.10/kWh. This suggests that the system presents a relatively costly alternative for refrigeration needs, higher than the conventional electricity costs at this specific COP value. However, as the COP rises, the LCOE proportionally decreases, indicating enhanced cost-effectiveness. At a COP of 0.65, the LCOE drops to $0.103/kWh. This establishes that the solar thermal absorption cooling system could be a viable and economical option when juxtaposed with the average electricity cost in the region. Lastly, at its peak efficiency with a COP of 0.8, the solar thermal absorption cooling system achieves a significantly reduced LCOE of $0.085/kWh, signifying substantial cost advantages in refrigeration operations compared to the prevalent regional electricity tariffs.

The NPV versus COP graph shown in Figure 24 represents the quantification of the present value of both cash inflows and outflows over the system's projected operational lifespan of 20 years while considering the time value of money discounted at an annual rate of 7.75%.

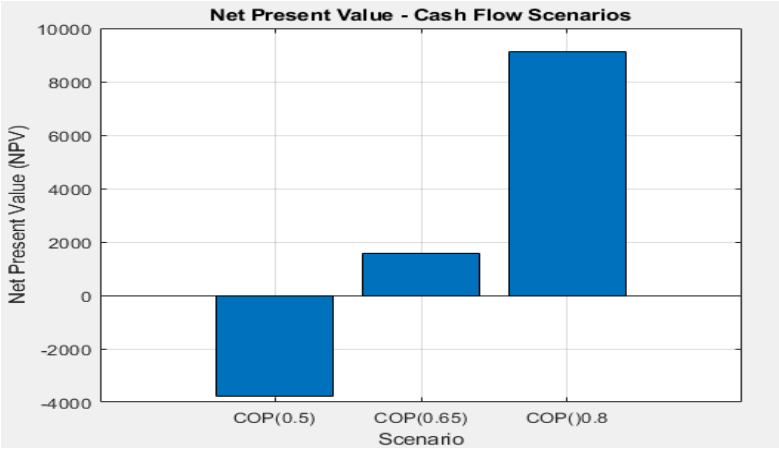

Figure 24. *NPV for different COP values (0.5, 0.65, and 0.8).*

When considering the solar thermal absorption cooling system with a COP of 0.5, the negative NPV of -$3,830 suggests a less favourable financial outlook. The negative NPV implies that the costs associated with the system including the initial investment and ongoing expenses exceed the expected benefits and cash inflows. Consequently, this indicates that the investment may not be financially attractive under these circumstances. Conversely, a COP of 0.65 demonstrates a positive NPV of $1,790, therefore suggesting a more favourable financial scenario. The positive NPV indicates that the benefits and cash inflows generated by the system outweigh the associated costs, resulting in a net positive value. This implies that the investment is expected to generate a profit and yield a satisfactory return on investment during the system's operational lifespan. Furthermore, for a COP of 0.8, the solar thermal absorption cooling system exhibits a significantly higher NPV of $9,200. This notable positive NPV underscores the enhanced profitability potential of the investment. The substantial positive NPV suggests that the expected cash inflows including energy cost savings and potential revenue streams surpass the costs by a substantial margin, indicating a financially lucrative investment opportunity.

The graph shown in Figure 25 indicates that for a COP of 0.5, the DPP is undefined as the cumulative discounted cash flows amount to -$3,768.5 in year 20. In contrast, for a COP of 0.65, the DPP was projected to be 18 years, while for a COP of 0.8, the DPP was projected to be 12 years considering the system's operational lifespan of 20 years.

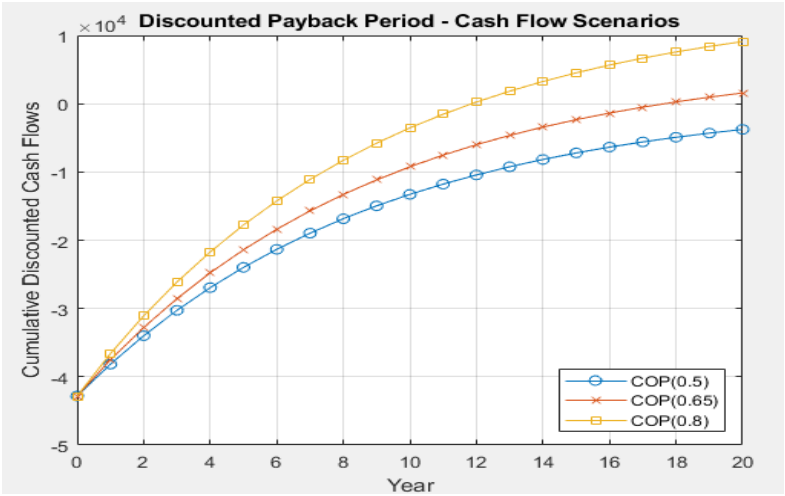

Figure 25. *DPP for different COP values (0.5, 0.65, and 0.8).*

The absence of a defined DPP for a COP of 0.5 signifies that the cumulative discounted cash flows fail to recover the initial investment within the 20-year time horizon. The negative

cumulative discounted cash flows of -$3,768.5 indicate that the system's cash outflows continue to exceed the discounted cash inflows throughout the entire duration. This finding raises concerns about the system's financial sustainability, suggesting an inability to recoup costs and generate positive returns within the specified timeframe. Conversely, a COP of 0.65 demonstrates a projected DPP of 18 years, indicating that the cumulative discounted cash flows from the solar thermal absorption cooling system are anticipated to surpass the initial investment within this timeframe. The positive DPP value suggests that the system achieves self-sufficiency and generates sufficient cash inflows to offset the discounted cash outflows by the end of the 18th year. This implies an eventual return on investment, although, not within a reasonable timeframe. However, for a COP of 0.8, the solar thermal absorption cooling system exhibits a relatively shorter DPP of 12 years. This implies that the system is expected to recover the initial investment and yield positive cumulative discounted cash flows within the initial 12 years of operation. This shorter DPP indicates a more accelerated return on investment for this specific COP scenario; it is closely similar to the pay-back period of 11 and 13.5 years found by Abed et al. for two scenarios in techno-economic analysis of solar-assisted combined absorption cooling cycle [50]. Their system design, with a cooling load of 5 kW and collector area and hot storage tank volume of 8.5 m^2 and 0.35 m^3 respectively, was also relatively comparable to the designed solar thermal absorption cooling system when the collector area was set to 12 m^2.

Within the context of a 20-year system lifespan shown in Figure 26, the SIR reaches 1 in year 17 for a COP of 0.5, year 15 for a COP of 0.65, and year 13 for a COP of 0.8.

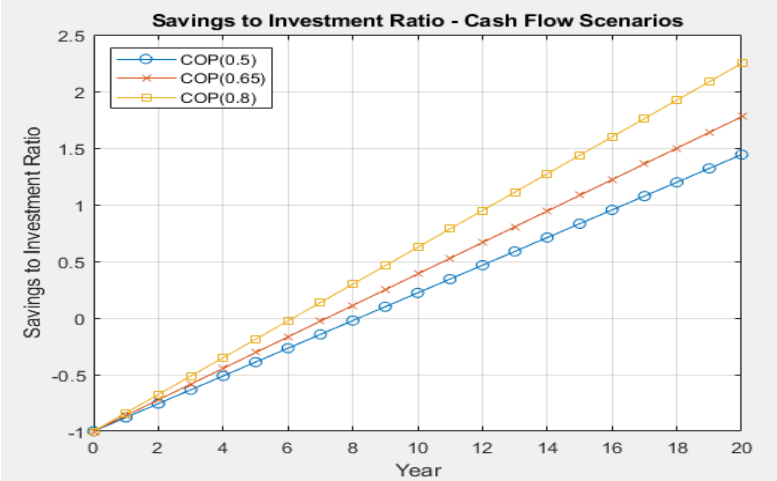

Figure 26. *SIR for different COP values (0.5, 0.65, and 0.8).*

For a COP of 0.5, the SIR reaching 1 in year 17 indicates that the cumulative savings gradually accumulate over the system's operational life, ultimately equalling the initial investment in the 17th year. The longer time required to achieve a SIR of 1 in this scenario can be attributed to the lower COP, which leads to slower savings accumulation and a comparatively delayed break-even point. While the investment eventually becomes financially sustainable, the extended recovery period raises concerns regarding the system's overall profitability and financial attractiveness. On the contrary, a COP of 0.65 demonstrates an earlier break-even point, with the SIR reaching 1 in year 15. The relatively higher COP contributes to more efficient energy utilization and cost savings, resulting in a faster recovery of the initial investment. This accelerated timeline indicates a favourable return on investment and enhances the system's financial prospects. Furthermore, the highest financial performance was observed with a COP of 0.8, where the SIR reached 1 in year 13. The system's superior energy efficiency driven by the higher COP facilitates significant cost savings and a more rapid recoupment of the initial investment. The shorter time to achieve a SIR of 1 underscores the system's enhanced financial profitability and strengthens its value proposition. This outcome emphasizes the advantages of investing in a system with a higher COP as it leads to faster savings accumulation and an earlier break-even point.

3.3 Optimal system design

The design of the optimal system starts with the choice of a chiller with a higher-rated COP value of 0.8, as it results in higher solar fraction values and greater utilization of solar energy for meeting the cooling load. Moreover, a larger collector area is opted for, as it leads to higher solar fraction values and increased solar thermal energy utilization. The optimal collector area of 12 m² allows for higher solar fraction and higher primary energy savings without costly collector oversizing. The optimal storage volume of 0.2 m^3 was selected to allow adequate thermal storage without much trade-off with the primary energy savings. This is because an increase in thermal storage requires more auxiliary energy to get the tank to hot water set-point temperature.

In consideration of economic metrics, The LCOE showed that the system achieved its lowest value at a rated COP of 0.8 with an LCOE of $0.085/kWh. This indicates that the STC system becomes more cost-effective as the COP increases, resulting in lower electricity production costs. The NPV analysis demonstrated the most favourable outcome for a COP of 0.8. At this COP, the NPV reached $9,200, indicating a significant positive value. This positive NPV implies that the benefits and cash inflows generated by the system outweigh the associated costs, making the investment financially lucrative. Regarding the DPP, the best performance was achieved with a COP of 0.8. The STC system exhibited a DPP of 12 years, indicating that the initial investment is expected to be recouped within this timeframe. This shorter DPP suggests a more rapid return on investment and enhances the financial feasibility of the system. Lastly, the SIR also highlighted the superior performance of the STC system at a COP of 0.8. The SIR reached 1 in year 13, indicating that the cumulative savings surpassed the initial investment within that timeframe. This accelerated break-even point further emphasizes the system's financial viability and attractiveness. Considering both technical and economic factors, the optimal system choice from all the parametric analyses involves a chiller with a COP value of 0.8, a collector area of 12 m², and a 0.5 m^3 hot storage volume. This combination maximizes the system's ability to meet a cooling load of 7.318 kW using solar energy. It also improves energy efficiency and offers cost-effective operation compared to conventional electricity costs.

4. Conclusions and recommendations

A comprehensive exploration was made of the history and challenges of food preservation and refrigeration, tracing the shift from ancient methods to modern refrigeration. A detailed literature review on solar thermal refrigeration was conducted, introducing its principles and components. Analysis was made on solar collectors, thermal storage, and the refrigeration cycle. STC technologies such as adsorption, absorption, and desiccant cooling were explored, emphasizing their principles and performance metrics. Mathematical models for these cooling technologies were presented. The methodology outlined a systematic approach to designing, simulating and economically analysing a STC system for fresh agricultural produce preservation in Lesotho. The choice of absorption cooling technology in modelling, its alignment with FAO recommended storage conditions and system simplicity were justified. TRNSYS was selected for simulation due to its transient system behaviour capabilities. Also, the geographical and temporal focus was explained. Furthermore, through the economic analysis, the simulation methodology, collector modelling, control strategies, and input specifics were described. Sensitivity analysis, essential for real-world uncertainties, outlined variations in collector efficiency, vegetable storage needs, and economic variables' impact on system performance and financial viability.

The results demonstrated the successful design and economic analysis of the cooling system. TRNSYS showed the system's efficiency in meeting cooling needs, emphasizing the significance of optimal sizing and hot storage volume on performance. The research demonstrates the effectiveness and economic viability of the designed STC system for preserving fresh agricultural produce. The economic impact analysis conducted using MATLAB provided

essential insights into the cost implications and financial feasibility of the system. Metrics such as LCOE, NPV, SIR and DPP were considered, revealing that a chiller with a higher-rated COP value of 0.8, a collector area of 12 m² and a hot storage volume of 0.2 m³ represents the optimal system design. This configuration maximizes solar energy utilization, resulting in higher solar fraction values and improved energy efficiency. It also offers cost-effective operation, with a lower LCOE of $0.085/kWh, a higher NPV of $9,200, a relatively short DPP of 12 years, and an early break-even point at year 13 according to the SIR analysis. These results underscore the financial feasibility and profitability of the STC system, making it an appealing investment option for refrigeration needs in the region. To enhance cost-effectiveness, it is recommended to consider larger-scale installations, invest in advanced materials and technologies, prioritize local manufacturing, explore government incentives and implement proactive maintenance. Additionally, long-term financing options and hybrid system integration can further improve affordability.

While this study is comprehensive, it is essential to acknowledge that for simplicity, parasitic electrical energy consumers such as fluid pumps, electronic sensors and lights were not accounted for. Recommendations for future research include exploring advanced optimization techniques such as machine learning algorithms for precise system parameter adjustments. This could boost overall performance. Also, developing dynamic models accommodating varying weather conditions and real-time demand fluctuations to enhance system reliability and accuracy. Moreover, conducting thorough analyses of market dynamics, policy frameworks, and regulatory incentives to assess readiness and potential obstacles for STC technology adoption.

Data availability statement

The results were not supported by any repository data as they emanate from mathematical modeling and software simulation.

Author contributions

Mpho Yengane: Investigation, Methodology, Software, Formal Analysis, Writing – original draft. **Sebota Mokeke:** Supervision, Validation, Writing – review & editing. **Moeketsi Mpholo:** Conceptualization, Project administration, Writing – review & editing.

Competing interests

The authors declare that they have no competing interests.

References

[1] R. C. Wiley, “Microbiological and Enzyme Considerations to Prevent Spoilage of MPR Fruits and Vegetables,” in Preservation Methods for Minimally Processed Refrigerated Fruits and Vegetables, 1994, p. 69. [Online]. Available: https://link.springer.com/chapter/10.1007/978-1-4615-2393-2_3

[2] O. Adekomaya, T. Jamiru, R. Sadiku, and Z. Huan, “Sustaining the shelf life of fresh food in cold chain – A burden on the environment,” Alexandria Engineering Journal, vol. 55, no. 2, pp. 1359–1365, Jun. 2016, doi: 10.1016/j.aej.2016.03.024.

[3] M. Khesa, C. Nhemachena, G. Matchaya, and S. Nhlengethwa, “Africa agriculture transformation scorecard performance and lessons for Lesotho,” Jul. 2019, Accessed: Jul. 28, 2022. [Online]. Available: https://cgspace.cgiar.org/handle/10568/105913

[4] Trading Economics, “Lesotho - Access To Electricity (% Of Population) - 2022 Data 2023 Forecast 1990-2020 Historical.” https://tradingeconomics.com/lesotho/access-to-electricity-percent-of-population-wb-data.html (accessed Nov. 24, 2022).
[5] L. Leistner, “Food preservation by combined methods,” Food Research International, vol. 25, no. 2, pp. 151–158, Jan. 1992, doi: 10.1016/0963-9969(92)90158-2.
[6] M. S. Tapia de Daza, S. M. Alzamora, J. W. Chanes, and G. Gould, “Combination of preservation factors applied to minimal processing of foods,” Critical Reviews in Food Science and Nutrition, vol. 36, no. 6, pp. 629–659, Jul. 1996, doi: 10.1080/10408399609527742.
[7] S. Rodgers, “Preserving non-fermented refrigerated foods with microbial cultures—a review,” Trends in Food Science & Technology, vol. 12, no. 8, pp. 276–284, Aug. 2001, doi: 10.1016/S0924-2244(01)00093-0.
[8] World Bank “Global Agricultural Trade and Developing Countries,” in Fruits and vegetables: global trade and competition in fresh and processed product markets, M. A. Aksoy and J. C. Beghin, Eds., The World Bank, 2004, p. 238. doi: 10.1596/0-8213-5863-4.
[9] H. M. Ali, “Recent advancements in PV cooling and efficiency enhancement integrating phase change materials based systems – A comprehensive review,” Solar Energy, vol. 197, pp. 163–198, Feb. 2020, doi: 10.1016/j.solener.2019.11.075.
[10] T. He, X Zhang, C. Wang, M. Wang, B. Li, N. Xue, K. Shimizu, K. Takahashi, Y. Wu, “Application of Solar Thermal Cooling System Driven by Low Temperature Heat Source in China,” Energy Procedia, vol. 70, pp. 454–461, May 2015, doi: 10.1016/j.egypro.2015.02.147.
[11] K. Saikia, M. Vallès, A. Fabregat, R. Saez, and D. Boer, “A bibliometric analysis of trends in solar cooling technology,” Solar Energy, vol. 199, pp. 100–114, Mar. 2020, doi: 10.1016/j.solener.2020.02.013.
[12] R. Best and N. Ortega, “Solar refrigeration and cooling,” Renewable Energy, vol. 16, no. 1–4, pp. 685–690, Jan. 1999, doi: 10.1016/S0960-1481(98)00252-3.
[13] A. Al-Alili, Y. Hwang, and R. Radermacher, “Review of solar thermal air conditioning technologies,” International Journal of Refrigeration, vol. 39, pp. 4–22, Mar. 2014, doi: 10.1016/j.ijrefrig.2013.11.028.
[14] T. Brosnan and D.-W. Sun, “Precooling techniques and applications for horticultural products Ð a review,” International Journal of Refrigeration, p. 17, 2001.
[15] D. J. Wuebbles and A. K. Jain, “Concerns about climate change and the role of fossil fuel use,” Fuel Processing Technology, vol. 71, no. 1–3, pp. 99–119, Jun. 2001, doi: 10.1016/S0378-3820(01)00139-4.
[16] N. Nkolisa, L. S. Magwaza, T. S. Workneh, and A. Chimphango, “Evaluating evaporative cooling system as an energy- free and cost- effective method for postharvest storage of tomatoes (Solanum lycopersicum L.) for smallholder farmers,” Scientia Horticulturae, vol. 241, pp. 131–143, Nov. 2018, doi: 10.1016/j.scienta.2018.06.079.
[17] T. Peters, “The clean cold chain in agriculture in developing countries,” Tropical Agriculture Association, United Kingdom, 36, Spring 2019. Accessed: Aug. 12, 2022. [Online]. Available: http://www.taa.org.uk
[18] M. G. Gado, S. Ookawara, S. Nada, and I. I. El-Sharkawy, “Hybrid sorption-vapor compression cooling systems: A comprehensive overview,” Renewable and Sustainable Energy Reviews, vol. 143, p. 110912, Jun. 2021, doi: 10.1016/j.rser.2021.110912.
[19] World Bank, “Transforming Lesotho’s Farmers into Entrepreneurs,” Oct. 2022. Accessed: Jul. 05, 2023. [Online]. Available: https://www.worldbank.org/en/news/feature/2022/10/13/transforming-lesotho-s-farmers-into-entrepreneurs
[20] International Trade Administration, “Lesotho - Agricultural Sector.” Accessed: Jul. 05, 2023. [Online]. Available: https://www.trade.gov/country-commercial-guides/lesotho-agricultural-sector
[21] T. A. Rantšo and M. Seboka, “Agriculture and food security in Lesotho: Government sponsored block farming programme in the Berea, Leribe and Maseru Districts,” Cogent Food & Agriculture, vol. 5, no. 1, p. 1657300, Jan. 2019, doi: 10.1080/23311932.2019.1657300.
[22] World Bank, “Solar resource maps of Lesotho,” SOLARGIS, 2020. https://solargis.com/maps-and-gis-data/download/lesotho (accessed Oct. 30, 2022).

[23] R. Z. Wang and X. Q. Zhai, “Development of solar thermal technologies in China,” Energy, vol. 35, no. 11, pp. 4407–4416, Nov. 2010, doi: 10.1016/j.energy.2009.04.005.
[24] K. R. Ullah, R. Saidur, H. W. Ping, R. K. Akikur, and N. H. Shuvo, “A review of solar thermal refrigeration and cooling methods,” Renewable and Sustainable Energy Reviews, vol. 24, pp. 499–513, Aug. 2013, doi: 10.1016/j.rser.2013.03.024.
[25] Lesotho Electricity and Water Authority (LEWA), “LEWA Annual Report 2021-2022,” Maseru, Lesotho, 2, Sep. 2021. Accessed: Jul. 29, 2022. [Online]. Available: http://www.lewa.org.ls/library
[26] International Energy Agency, “Financing Clean Energy in Africa – Analysis - World Energy Outlook Special Report 2022,” IEA. Accessed: Oct. 19, 2023. [Online]. Available: https://www.iea.org/reports/financing-clean-energy-in-africa
[27] Lesotho Department of Energy, “Support to the Energy Sector Reform in Lesotho: Technical Guidelines for Off-Grid Products,” Department of Energy Lesotho. Accessed: Feb. 15, 2024. [Online]. Available: https://www.doe.gov.ls/post/view/59
[28] Y. Yu and E. C. Jaenicke, “Estimating Food Waste as Household Production Inefficiency,” American J Agri Economics, vol. 102, no. 2, pp. 525–547, Mar. 2020, doi: 10.1002/ajae.12036.
[29] FAO, “Manual for the preparation and sale of fruits and vegetables,” FAO.ORG. Accessed: Nov. 10, 2022. [Online]. Available: https://www.fao.org/3/y4893e/y4893e06.htm
[30] A. Ghafoor and A. Munir, “Worldwide overview of solar thermal cooling technologies,” Renewable and Sustainable Energy Reviews, vol. 43, pp. 763–774, Mar. 2015, doi: 10.1016/j.rser.2014.11.073.
[31] R. L. Shrivastava, V. Kumar, and S. P. Untawale, “Modeling and simulation of solar water heater: A TRNSYS perspective,” Renewable and Sustainable Energy Reviews, vol. 67, no. 3, pp. 126–143, 2017, doi: 10.1016/j.rser.2016.09.005.
[32] TRNSYS, “Welcome | TRNSYS : Transient System Simulation Tool,” TRNSYS. Accessed: Oct. 31, 2022. [Online]. Available: https://www.trnsys.com/
[33] Lesotho Meteorological Services, “Climate of Lesotho,” 2023. https://www.lesmet.org.ls/home/open/Climate-of-Lesotho (accessed Jul. 18, 2023).
[34] J. Asadi, P. Amani, M. Amani, A. Kasaeian, and M. Bahiraei, “Thermo-economic analysis and multi-objective optimization of absorption cooling system driven by various solar collectors,” Energy Conversion and Management, vol. 173, pp. 715–727, Oct. 2018, doi: 10.1016/j.enconman.2018.08.013.
[35] worlddata.info, “Climate comparison: Lesotho / Orange Free State,” Worlddata.info, 2023. https://www.worlddata.info/climate-comparison.php?r1=lesotho&r2=za-orange-free-state (accessed Apr. 11, 2023).
[36] QAiST (Quality Assurance in Solar Heating and Cooling Technology), “Topic report for WP2 Solar thermal collectors (Performance testing of evacuated tubular collectors),” no. 2.1, 2012.
[37] K. K. Gopinathan, “Solar radiation on variously oriented sloping surfaces,” Solar Energy, vol. 47, no. 3, pp. 173–179, 1991, doi: 10.1016/0038-092X(91)90076-9.
[38] M. S. A. Khan, A. W. Badar, T. Talha, M. W. Khan, and F. S. Butt, “Configuration based modeling and performance analysis of single effect solar absorption cooling system in TRNSYS,” Energy Conversion and Management, vol. 157, pp. 351–363, Feb. 2018, doi: 10.1016/j.enconman.2017.12.024.
[39] D. Milani, “Renewable Energy Integration in Combined Cooling, Heating, and Power (CCHP) Processes,” in Polygeneration with Polystorage for Chemical and Energy Hubs, Elsevier, 2019, pp. 459–491. doi: 10.1016/B978-0-12-813306-4.00014-8.
[40] Trading Economics, “Lesotho Interest Rate - 2023 Data - 1980-2022 Historical - 2024 Forecast - Calendar,” 2023. https://tradingeconomics.com/lesotho/interest-rate (accessed Jul. 18, 2023).
[41] B. Epp, “IEA SHC: Levelised Cost of Heat and the Calculations behind It,” Solarthermalworld. Accessed: Feb. 28, 2024. [Online]. Available: https://solarthermalworld.org/news/iea-shc-levelised-cost-heat-and-calculations-behind-it/

[42] Lesotho Electricity and Water Authority (LEWA), “Approved Electricity Tariffs & Charges,” Lesotho Electricity and Water Authority, 2022. https://www.lewa.org.ls/approved-electricity-tariffs-charges/ (accessed Jul. 09, 2023).
[43] B. M. Taele, L. Mokhutšoane, I. Hapazari, S. B. Tlali, and M. Senatla, “Grid electrification challenges, photovoltaic electrification progress and energy sustainability in Lesotho,” Renewable and Sustainable Energy Reviews, vol. 16, no. 1, pp. 973–980, Jan. 2012, doi: 10.1016/j.rser.2011.09.019.
[44] T. Sokhansefat, D. Mohammadi, A. Kasaeian, and A. R. Mahmoudi, “Simulation and parametric study of a 5-ton solar absorption cooling system in Tehran,” Energy Conversion and Management, vol. 148, pp. 339–351, Sep. 2017, doi: 10.1016/j.enconman.2017.05.070.
[45] İ. Uçkan and A. A. Yousif, “Investigation of the effect of various solar collector types on a solar absorption cooling system,” Energy Sources, Part A: Recovery, Utilization, and Environmental Effects, vol. 43, no. 7, pp. 875–892, Apr. 2021, doi: 10.1080/15567036.2020.1766599.
[46] U. Eicker and D. Pietruschka, “Design and performance of solar powered absorption cooling systems in office buildings,” Energy and Buildings, vol. 41, no. 1, pp. 81–91, Jan. 2009, doi: 10.1016/j.enbuild.2008.07.015.
[47] R. Figaj, M. Szubel, E. Przenzak, and M. Filipowicz, “Feasibility of a small-scale hybrid dish/flat-plate solar collector system as a heat source for an absorption cooling unit,” Applied Thermal Engineering, vol. 163, p. 114399, Dec. 2019, doi: 10.1016/j.applthermaleng.2019.114399.
[48] J. Aman, D. S.-K. Ting, and P. Henshaw, “Residential solar air conditioning: Energy and exergy analyses of an ammonia–water absorption cooling system,” Applied Thermal Engineering, vol. 62, no. 2, pp. 424–432, Jan. 2014, doi: 10.1016/j.applthermaleng.2013.10.006.
[49] O. Ayadi and S. Al-Dahidi, “Comparison of solar thermal and solar electric space heating and cooling systems for buildings in different climatic regions,” Solar Energy, vol. 188, pp. 545–560, Aug. 2019, doi: 10.1016/j.solener.2019.06.033.
[50] A. M. Abed et al., “Techno-Economic Analysis of dual ejectors solar assisted combined absorption cooling cycle,” Case Studies in Thermal Engineering, vol. 39, p. 102423, Nov. 2022, doi: 10.1016/j.csite.2022.102423.